MIGRATORY TRANSITIONS AND ONCOGENIC TRANSFORMATION IN EPITHELIAL CELLS ARE CONTROLLED BY THE THRESHOLD OF THE RAS/PI3K/ERK EXCITABLE NETWORK

By

Huiwang Zhan

A dissertation submitted to Johns Hopkins University in conformity with the requirements for the degree of Doctor of Philosophy.

Baltimore, Maryland

January 2020

Abstract

The Ras/PI3K/ERK signaling network plays fundamental roles in cell growth, survival, and migration and is frequently activated in cancer. Here we show that the activities of the signaling network propagate as coordinated waves, biased by epidermal growth factor, which drive actin-based protrusions in human epithelial cells. The network exhibits other key hallmarks of biochemical excitability, including annihilation of oppositely directed waves, all-or-none responsiveness, and refractoriness to repeated stimuli. Abrupt perturbations to Ras, PI(4,5)P2, PI(3,4)P2, ERK, and TORC2 alter the threshold for network activation, observations which define positive and negative feedback loops within the network. Importantly, oncogenic transformation dramatically increases coupled signal transduction and cytoskeletal wave activity, the frequency of ERK pulses, and the sensitivity to EGF stimuli. The view that oncogenic transformation is a shift to a lower threshold or set point of excitable Ras/PI3K/ERK network, caused by various combinations of genetic insults, can facilitate assessment of cancer severity and the effectiveness of interventions.

Advisers: Peter N. Devreotes and Chuan-Hsiang Huang

Reader: Pablo A. Iglesias

Acknowledgements

I would like to thank my excellent mentors Peter N. Devreotes, Chuan-Hsiang Huang, and Pablo A. Iglesias. I would like to thank Sayak Bhattacharya for the computational simulation work (Figure 4G and 4H), Huaqing Cai for Kras_G12V recruitment experiment (Figure 14A), Pablo A. Iglesias for the kymograph of cell lamellipodia length (Figure 7B), and Yuchuan Miao for the previous work in *Dictyostelium*. I sincerely thank my former and current thesis committee members, including King-Wai Yau, Andrew Ewald, Pierre Coulombe (currently at the University of Michigan), and Duojia Pan (currently at the University of Texas Southwestern Medical Center). I sincerely thank the great support from Biological Chemistry Program and the former and current program directors Michael Caterina, Denise Montell, Natasha Zachara, and Stephen Gould, as well as the program coordinator Darlene Sutton. I appreciate helpful suggestions and discussions from all members of the laboratories of Peter Devreotes, Chuan-Hsiang Huang, Pablo Iglesias, Douglas Robinson, and Miho Iijima. I would like to thank Yuchuan Miao and Mingjie Wang for the guidance when I initially joined the lab. And I appreciate all the support from the Departments of Cell Biology, Biological Chemistry and the JHMI Microscope Facility.

I also thank Dr. Schmidt of Wolfgang Losert laboratory (University of Maryland) for writing the Matlab script for analysis of ERK-KTR changes. I thank Takanari Inoue (JHU), Stephen Desiderio (JHU) and Balla (NIH) laboratories and Addgene for generous provision of plasmids and Miho Iijima and Jun Liu laboratories for generous provision of cells. The thesis work was supported by NIH grant R35 GM118177 (to P.N.D.), AFOSR MURI FA95501610052 (to P.N.D.), DARPA HR0011-16-C-0139 (to P.N.D. and P.A.I.), K22CA212060 (to C.H.H.), a Cervical Cancer SPORE

P50CA098252 Career Development and Pilot Project Awards (to C.H.H.) and NIH Grant S10 OD016374 (to S. Kuo of the JHMI Microscope Facility).

Last but not least, I would like to thank the enormous supports and understanding from my family and friends especially my parents Linrong Zhan and Yuxiang Zhou and my girlfriend Qunqi Tian.

Table of Contents

List of Figures

Introduction

1. Fundamentality of Cell Migration in Biology and Health

Cell migration is one of the most crucial processes in many biological and physiological events such as development, wound healing, immune response and cancer metastasis. Understanding cell migration is not only critical for knowing the mechanism of one of the most basic and fundamental life science questions, but also indispensable for developing therapeutic strategies towards many human diseases (Manahan et al., 2004; Swaney et al., 2010; Devreotes et al., 2017).

Cells are able to sense, incorporate, and migrate to a variety of biochemical and biophysical cues including chemicals (**chemotaxis** for soluble chemicals and **haptotaxis** for surface attached chemicals) (Carter et al., 1965; Jeon et al., 2002; Helmick et al., 2008; Bray et al., 2000; Bagorda & Parent 2008; Tessier-Lavigne 1994), rigidity of the substrate (**mechanotaxis** or **durotaxis**) (Lo et al., 2000; Cortese et al., 2009; Palamà et al., 2012;), extracellular tension (**tensotaxis**) (Beloussov et al., 2000;), topographical surface features (**contact guidance**) (Curtis et al., 2001; Dalby et al., 2007; Cortese et al., 2009), electric fields (**electrotaxis** or **galvanotaxis**) (Erickson et al., 1984; Cortese et al. 2014, Gao et al. 2011; Zhao et al. 2006), **temperature** (Ramot et al. 2008; Whitaker & Poff 1980), light (**phototaxis)** (Saranak et al., 1997; Armitage& Hellingwerf 2003), and gravitational potential (**geotaxis**) (Adams et al., 1999). Cell can also take into account and migrate in the presence of several different types of cues (Hale et al., 2010). Among these different forms of directed cell migrations, chemotaxis is the most common type happening in human body and is by far the most extensively studied.

One common mechanism for the migration of most eukaryotic cells is by forming actin-filled protrusions (also known as projections) at the front and actomyosin-based contraction at the rear of the cell or at the base of the projections. The extension of protrusions at the front and retracting activities at the back of the cell are also well coordinated with the attachment and detachment to the substrate by assembling and disassembling the adhesion components. As diversity is a core character of biological events, the formation of protrusions is quite dynamic and various in living cells. These morphologically different protrusion modes typically seen in most eukaryotic cells are lamellipodia, macropinosomes, pseudopods and blebs. Different cells use different types of protrusions. One cell can utilize and switch within various types of migratory modes, which – if not properly regulated – underlies severe diseases such as the cancer metastasis (Devreotes et al., 2017; Blaser et al., 2006; Yoshida & Soldati 2006; Fackler & Grosse 2008; Wolf et al., 2003; Richardson & Lehmann 2010; Barnhart et al., 2010; Keren & Theriot 2008; Shaw & Martin 2009; Baumann 2014; Wright et al., 2001; Lakshman & Finn 2001; Moulding et al., 2013; Condeelis et al., 2005; Reymond et al., 2013; Neumann et al., 2018).

2. Excitable Network Hypothesis in *Dictyostelium* Cells

Studies of the signal transduction and cytoskeletal events involved in rapid morphological changes primarily in *Dictyostelium* cells have led to the "excitable network hypothesis". It proposes that self-organizing signal transduction activities at the cell cortex provide global control of acto-myosin based protrusions that underlie cell dynamics. The signaling and cytoskeletal networks are excitable. External chemical and biomechanical stimuli can guide cells and be integrated by influencing the overall threshold or set-point of the network. Altering the threshold of these

networks generates diverse patterns of activity, leading to the varied protrusions, such as lamellipodia and filopodia, exhibited by cells (Gerisch et al., 2004; Weiner et al., 2007; Arai et al., 2010; Huang et al., 2013; Taniguchi et al., 2013; Nishikawa et al., 2014; Tang et al., 2014; Miao et al., 2017; Yang et al., 2018).

Among the patterns that excitable systems can display are propagating waves on two-dimensional surfaces. Travelling actin waves were initially discovered in *Dictyostelium* cells and the features of these waves have been extensively investigated (Vicker et al., 2002; Inagaki et al., 2017). Evidence suggests the waves of cytoskeletal activity are driven by signal transduction events which involve Ras family proteins and phosphoinositide 3-kinases (PI3Ks). The Ras-PI3K signal transduction excitable network (STEN) couples to the cytoskeletal excitable network (CEN) to control cell migration (Huang et al., 2013; Miao et al., 2017; Miao et al., 2019).

In addition to the traveling waves, further studies in *Dictyostelium* have provided direct evidence for biochemical excitability (Huang et al., 2013). Cytoskeletal and signal transduction responses display “all-or-nothing” behavior to stimuli. A full response to the second stimulus can only be triggered after certain length of interval, proving the existence of refractory period. Refractory periods are consistent with the observed annihilation of oppositely directed waves (Gerisch et al., 2004).

In *Dictyostelium*, lowering or raising the threshold of the Ras-PI3K network altered cellular protrusions and the mode of cell migration (Miao et al., 2017; Miao et al., 2019). These observations contributed to a molecular model of the feedback loops involving Ras, PI3K, TORC2, PKB, PI5K et al, which lead to excitability. Transitions between protrusion types and migration

modes were closely simulated with models of coupled excitable signal transduction and cytoskeletal networks.

3. Excitability of Signal Transduction Network in Mammalian Cells

There are no in depth studies on "excitable network hypothesis" in controlling the morphology and migration of mammalian cells, despite some indirect evidences from several cell types indicating the presence of some properties of "excitability".

Firstly, travelling waves of cytoskeletal activities have been observed in a variety of mammalian cells. Waves of SCAR/WAVE and F-actin steer the movement of neutrophils (Weiner et al., 2007; Wang et al., 2014; Yang et al., 2016). Additional examples include F-actin waves in mast cells (Wu et al., 2018), in spreading lymphocytes and macrophages (Lam Hui et al., 2014), in breast cancer cells (Marchesin et al., 2015), in Xenopus oocytes (Bement et al., 2015), and in extending neuronal axons (Winans et al., 2016) and integrin waves in osteosarcoma cells (Case et al., 2011). Whether there are similar travelling signaling waves upstream such as Ras-PI3K is not clear, even though wave-like protrusions bearing activated Ras and PIP3 have been observed in fibroblasts, neutrophils, and cancer cells (Wozniak et al., 2005; Welf et al., 2012; Wang et al., 2014; Yang et al., 2018;). Therefore, it is not known whether these cytoskeletal waves are coupled with and controlled by upstream excitable signaling networks, and how these cells respond to acute alterations of these networks remains to be tested.

Secondly, in neutrophils, cytoskeletal and signal transduction responses display features of threshold and refractory period (Tang et al., 2014), and two colliding Hem-1 (component of the WAVE2 complex) waves annihilate (Weiner et al., 2007). One of the cell types studied here, the

human mammary epithelial cell line, MCF-10A, displays oscillatory ERK activity which can be phase-shifted by exogenous EGF, and displays adaptive behavior, typical properties of an excitable network (Albeck et al., 2013). However, these features of excitability have not been tested in the majority of cells displaying cytoskeletal waves. The extent to which excitable networks with similar molecular architecture are operating in human and mammalian cells remains to be determined.

4. The Complexity of Signaling Networks Leading to Cancer

Elucidating the quantitative properties of the signaling networks controlling cell morphology is critical for understanding and treating diseases such as cancer. The Ras/PI3K/ERK signaling networks are frequently mutated in cancer and this leads to oncogenic transformation (Basolo et al., 1991; Imbalzano et al., 2009; Liu et al., 2009). It is known that the excess activation of a single oncogene such as KRas is able to trigger hundreds of protein interactions and signaling feedback loops during transformation (Ye et al., 2016; Martinko et al., 2018).

However, there is a lack of systems-level understanding of how these interactions and feedback loops are intrinsically regulated, which largely explains the poor outcome of clinical practices that target various single components of the signaling networks (Lito et al., 2013; Simanshu et al., 2017). RTK-RAS-RAF-ERK is one canonical pathway that regulates cancer progression. As shown in Figure 1, complex positive and negative feedback loops coordinate the dynamic behavior of this signal transduction pathway (Shin et al., 2009; Lito et al., 2013; Simanshu et al., 2017). Activating BRAF mutations, such as BRAF_V600E, are present in ~70% of primary melanomas, ~10% of colorectal cancers and 30~70% of papillary thyroid carcinomas. Highly selective

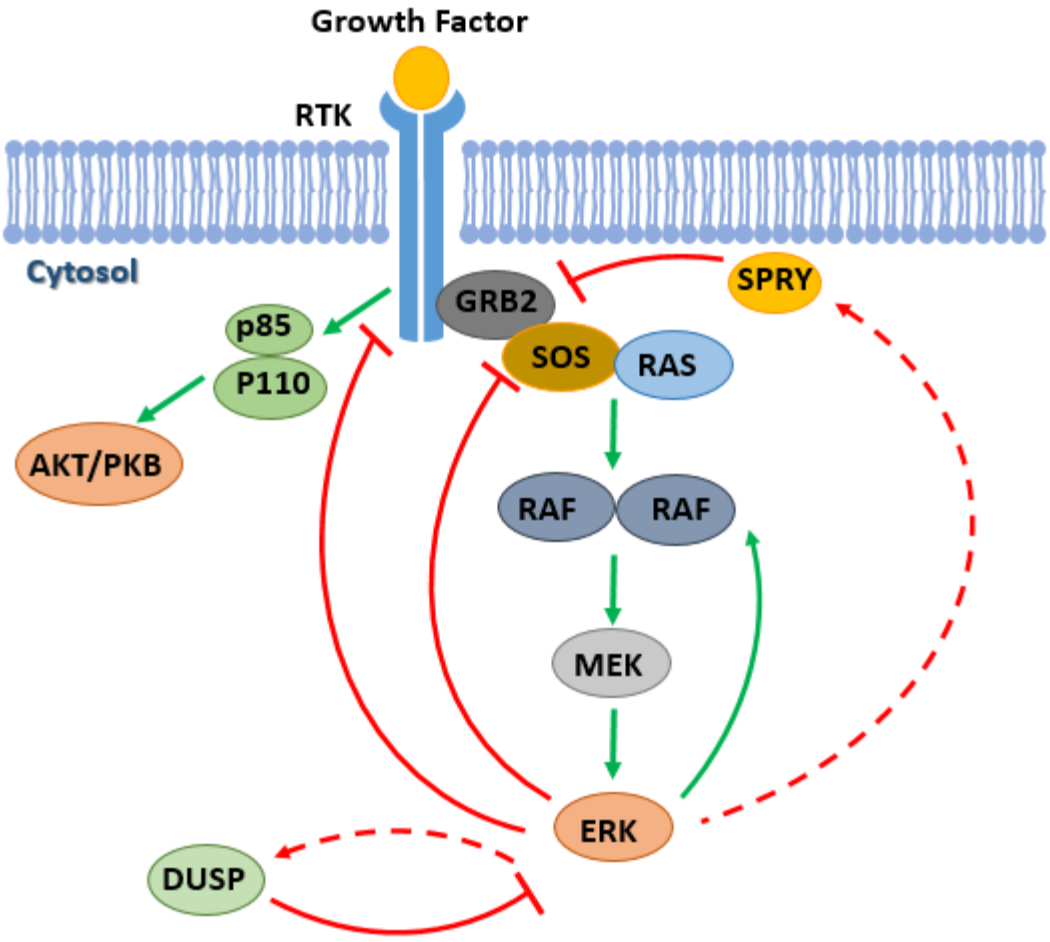

Figure 1. Positive and negative feedback loops regulate the complexity of RTK-RAS-RAF-ERK pathway.

Green arrows indicate activating interactions, red bars indicate inhibitory interactions, and red dashed arrows indicate activation through transcriptional expression. RTK (such as EGFR) on the cell membrane activates PI3K and Ras when bound to growth factors (such as EGF). PI3K later activates downstream factor AKT to trigger cell response such as proliferation. Active Ras triggers the activation of MAP kinases such as ERK through a series of phosphorylation reactions. Activation of this pathway causes progression of many diseases especially cancer. ERK can further activate this signaling pathway by forming a positive feedback to RAF. On the other hand, ERK is responsible for forming many negative feedback loops to RTK, GRB2, SOS, and ERK itself to prevent the signaling from excessive turn-on, which significantly accounts for

(Continued)

the adaptation mechanism of this pathway. SPRY and DUSP are proteins that are transcriptionally expressed after the activation of ERK. SPRY impairs signaling by disrupting the GRB2-SOS interaction and DUSP is an ERK-specific phosphatase. Diagram is modified from Shin et al., 2009; Lito et al., 2013; and Simanshu et al., 2017.

BRAF_V600E inhibitor vemurafenib (PLX4032) was effective in the treatment of BRAF-mutant melanomas (~80% response rate) but not in BRAF-mutant colorectal cancers (~5% response rate) or thyroid carcinomas (Corcoran et al., 2012; Prahallad et al., 2012; Lito et al., 2013). It is shown that the insensitivity and acquired resistance to BRAF inhibitor was partially due to the reactivation of ERK by feedback from RTK receptors, mainly EGFR in colorectal cancers and HER3 in thyroid cancers. Melanoma cells have less expression of EGFR, less reactivation of ERK and thus higher response rate to vemurafenib. Similarly, it was newly reported that individual lung cancer cells have rapid non-uniform adaptation to KRAS_G12C inhibitor by expressing new KRAS_G12C and activating epidermal growth factor receptor and aurora kinase signaling (Xue et al., 2020). There are also many other mechanisms and hypothesis proposed accounting for the adaptation of tumors to inhibitors of this pathway (Lito et al., 2013). These observations have demonstrated the complexity of the signaling events leading to cancer and called on new thoughts on the intrinsic property of these signaling networks.

These considerations prompted us to investigate the excitable properties of the Ras/PI3K/ERK network in human epithelial cells, and the role of excitability in oncogenic transformation. We surveyed a series of mammalian cell lines and found that MDA-MB-231, a breast cancer cell line,

displayed traveling Ras-PI3K-F-actin waves on the basal surface. We examined MDA-MB-231 cells and non-tumorigenic mammary cell line MCF-10A for evidence of biochemical excitability and the capacity of perturbations to alter these events and cellular protrusions. Both cell lines displayed all-or-nothing responsiveness and refractory periods. External stimuli and acute synthetic perturbations altered wave and/or protrusion behaviors as well as ERK pulse frequency. These observations allowed us to delineate the feedback loops that bring about excitability. Furthermore, activation of Ras enhanced wave activity in MDA-MB-231 cells, triggered *de novo* wave activity in MCF-10A cells, and increased protrusions in both. Taken together, these studies suggest that excitable Ras/PI3K/ERK network as driver of cellular protrusions is a general property of migrating cells and that cellular transformation can be considered as a shift to a lower threshold or set point of these networks.

Results

1. Coupled Signal Transduction and Cytoskeleton Waves Drive Protrusions

To monitor signal transduction and cytoskeleton activities at the ventral surface of MDA-MB-231 cells, we co-expressed biosensors for F-actin (Lifeact) and PIP3 (PH-AKT). As shown in Figure 2A, the signal transduction and cytoskeleton activities initiated spontaneously and propagated as waves along the basal membrane. The activities were highly coordinated; the leading edge and peak of the actin and PIP3 waves coincided. Whereas the cytoskeletal wave was confined to 5 μm, the lagging edge of the signal transduction wave was broader (Figure 2B). Similarly, as the waves passed, the signal transduction and cytoskeleton activities initially increased in parallel and peaked at about 5 min. The cytoskeletal activity returned to basal within about 5 min while signal transduction activity lasted longer (Figure 2C). The velocity of the travelling waves was 1.36 ± 0.22 μm/min (mean ± SD, n = 20) (Figure 2D). Many of the coupled F-actin and PIP3 waves started within the ventral surface and died out before reaching the edge of these large cells. The maximal lateral expansion of the waves was 20.05 ± 7.51 μm (mean ± SD, n = 20) with a duration of 24.20 ± 8.43 min (mean ± SD, n = 20) (Figure 2E and 2F). When a wave reached the edge of the cell, a ruffle strongly labeled with LifeAct and PH-AKT formed. This suggests that protrusions in epithelial cells are driven by coordinated PIP3/F-actin waves (Figure 2G).

In some instances, travelling waves stopped their forward progression and “hovered” in place. Figure 2H shows an example of a PIP3 wave which displayed some dynamic changes but did not propagate laterally for about 12 min. Then the wave began to propagate and continued for about 12 min before it stopped again. After about 8 min, it started to propagate again.

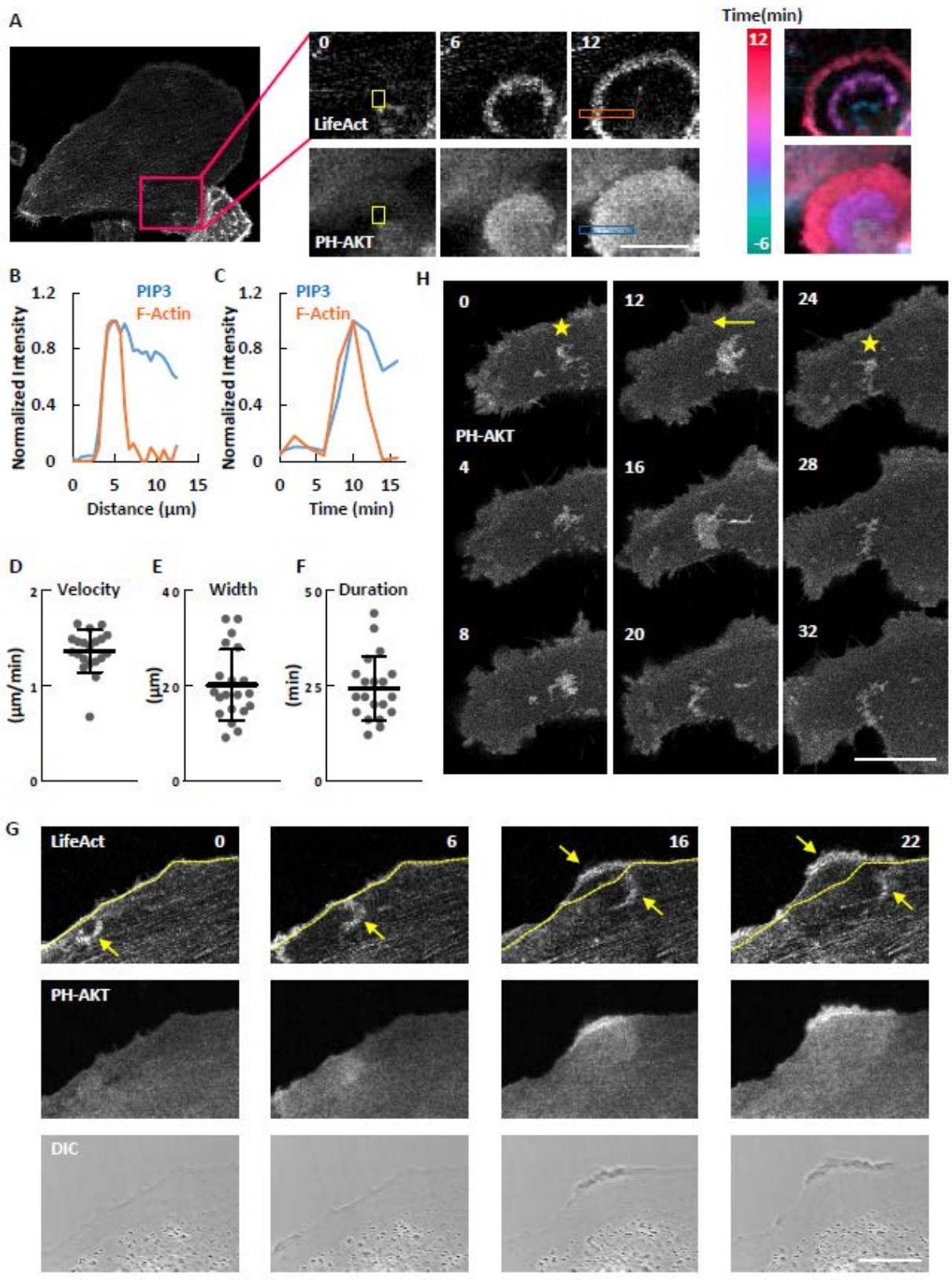

Figure 2. Cytoskeletal and signaling waves on the basal surface of MDA-MB-231 cells.

(Continued)

(A) Confocal images of MDA-MB-231 cells expressing biosensors for F-actin (LifeAct-RFP) and PIP3 (PH-AKT-GFP). Color-coded overlays show progression of waves as a function of time.

(B) Relative amount of F-actin and PIP3 across the orange and blue boxes scan in (A).

(C) Temporal change of F-actin and PIP3 in the yellow boxes in (A).

(D-F) Distribution of the velocity (D), maximum width (E) and duration (F) among waves (mean ± S.D. of N = 20 waves).

(G) Example of a circular wave with one edge propagating outwards to drive the formation of a protrusion upon reaching the cell perimeter (arrow indicates wave and dashed line indicates initial cell perimeter).

(H) Time-lapse confocal images of PH-AKT showing transitions between standing (marked with star) and travelling (marked with arrow) waves. The unit of time labeled on images is min and scale bar is 20 μm (same for the later figures).

2. Signal Transduction and Cytoskeletal Networks are Excitable

Previous studies in migrating *Dictyostelium* amoebae demonstrated that signal transduction and cytoskeletal activities display features of excitable systems including mutually annihilating waves, all-or-none responses, and the existence of a refractory period (Gerisch et al., 2004; Huang et al., 2013). Some of these features were also observed in human neutrophils (Weiner et al., 2007; Tang et al., 2014). The following results indicate that an excitable system underlies the signaling and cytoskeletal waves in MDA-MB-231. First, when two oppositely propagating waves of Lifeact merged (3.5 min in Figure 3A upper panel), they did not cross, but instead merged and disappeared (7.1 and 10.6 min in Figure 3A upper panel). Similar annihilation was also observed for colliding waves of PH-AKT (Figure 3A lower panel).

Second, we examined PIP3 production in response to EGF stimuli of increasing duration. MCF-10A cells responded to 1 and 5 min stimuli but rarely to a 30 sec stimulus (Figure 3B). Moreover, the magnitude and kinetics of the average responses to 1 or 5 min stimuli were nearly identical (Figure 3B and 3C). A similar duration threshold was obtained in MDA-MB-231 cells (Figure 3D and 3E). These observations suggested that stimuli crossing a threshold can trigger full responses. Third, we applied paired 1 min stimuli separated by various intervals. The second stimulus failed to trigger a full response unless a sufficient recovery time was allowed, suggesting the existence of a refractory period (Figure 3F and 3G). In both cell types, the kinetics of the recovery showed an initial lag of about 10 min, and the magnitude of the second response was half maximal after 25 min of recovery. Taken together, these observations indicate that cytoskeletal and signaling activities in MCF-10A and MDA-MB-231 cells indeed display salient features of excitable systems.

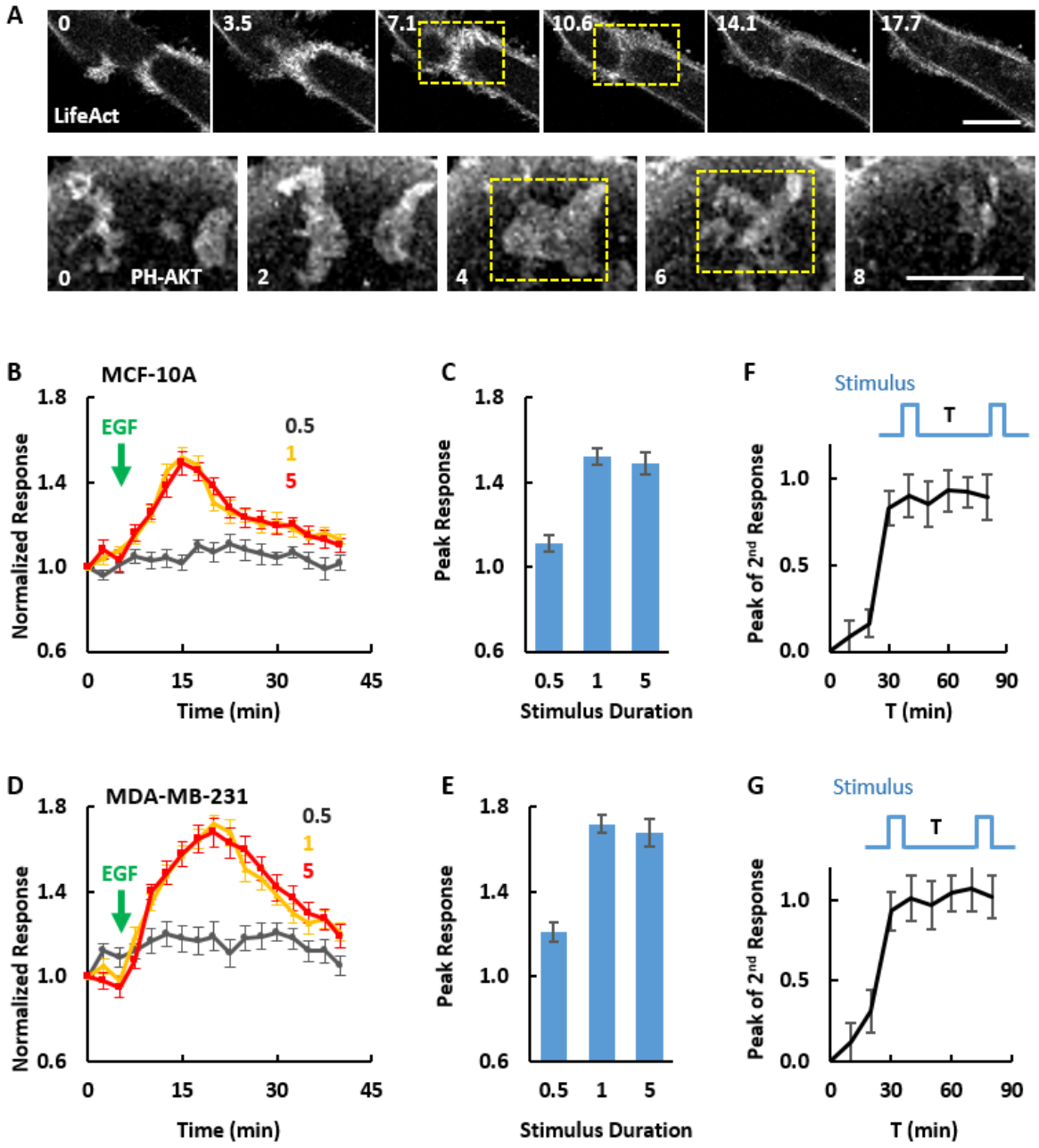

Figure 3. Excitability of the signaling network.

(A) Two colliding actin or PIP3 waves in MDA-MB-231 cells annihilated (dashed yellow boxes).

(B-E) Quantification of PIP3 responses to 0.5, 1 and 5 min EGF stimuli in MCF-10A (B and C) and MDA-MB-231 (D and E) cells (mean ± S.E.M. of n = 10 cells).

(Continued)

(F and G) Peak responses to the second of two 1 min stimuli separated by interval T in MCF-10A (F) and MDA-MB-231 (G) cells (mean ± S.E.M. of n = 10 cells).

3. Exogenous EGF Perturbs Signal Transduction and Cytoskeletal Waves

We examined the effects of uniform and gradient EGF stimuli on wave behavior. When a MDA-MB-231 cell was given a uniform EGF stimulus, the coupled F-actin and PIP3 waves initially disappeared and were replaced by a bright ring of signal around the cell perimeter. After about 50 min, waves began to reappear in the central region as the edge signal decreased (Figure 4A and 4B). Eventually they were more prevalent than those in cell prior to stimulation. The temporal evolution of the responses over the peripheral and interior regions was evident in kymographs of cropped images (Huang et al., 2013) (Figure 4C). We next used an EGF-filled micropipette to generate a spatial gradient of stimulation. At the steady state, PH-AKT waves that formed toward the high side of the EGF gradient were wider, more intense, and longer-lasting than those closer to the low side of the gradient (Figure 4D-F).

Building on a previously published mathematical model of the excitable signaling network (Xiong et al., 2010), we were able to simulate the responses of cells to uniform and gradient stimuli. In the two-dimensional simulation, prior to stimulation, spontaneous waves were triggered by noise. A uniform stimulus induced a global response followed by a brief period of inactivity before the waves were reinitiated (Figure 4G). These results are generally in agreement with the observed responses in MDA-MB-231 cells except that the global response in live cells was primarily seen at the perimeter rather than across the basal surface (Figure 4A). With a gradient stimulus, more abundant and wider waves were generated close to the high side of the gradient (Figure 4H), consistent with the observations in Figure 4D.

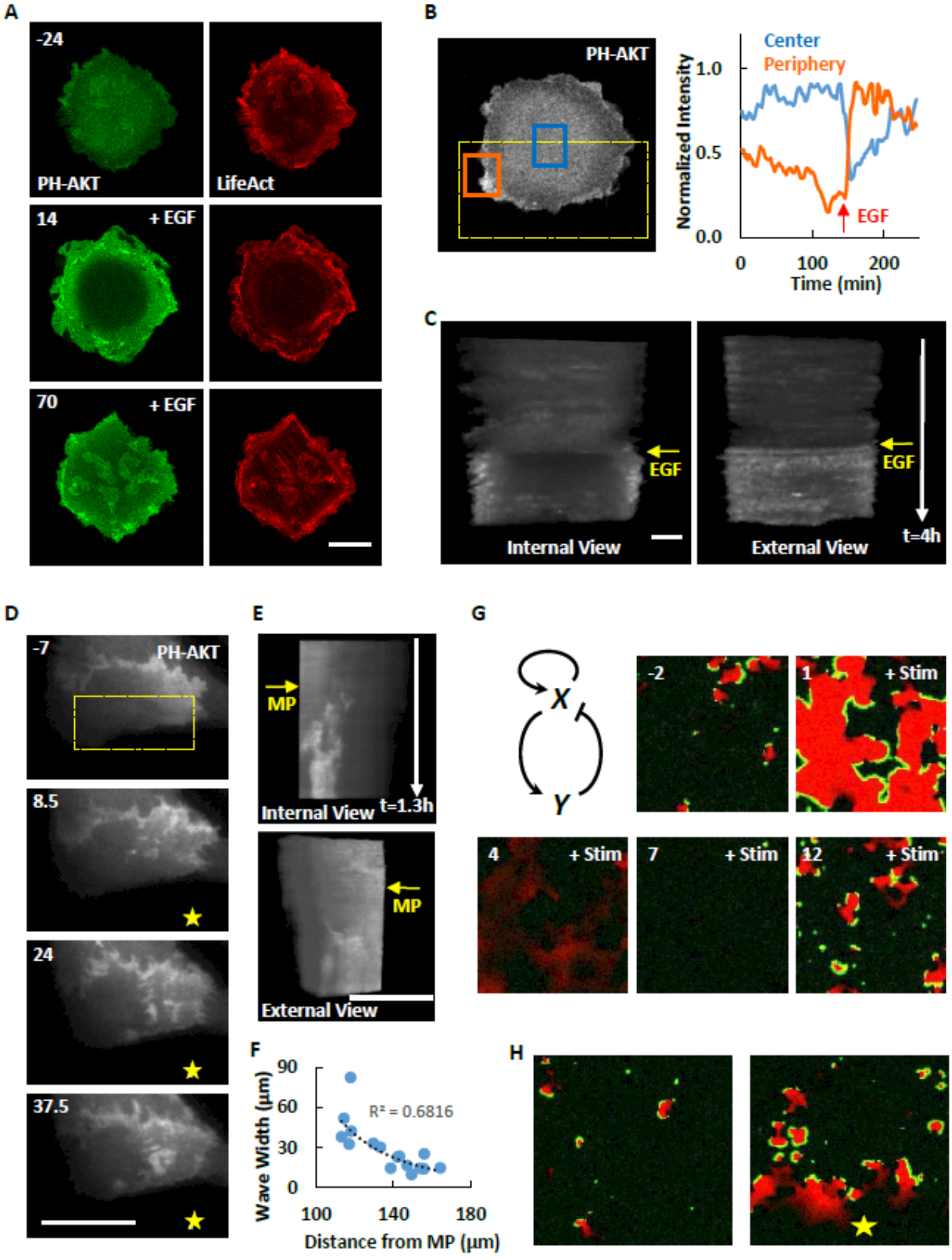

Figure 4. Responses of cytoskeletal and signaling waves to stimuli.

(Continued)

(A) Response of PIP3 and actin waves to global EGF stimulation (2 ng/ml, added at 0 min).

(B) Quantification of PIP3 change at the center (blue box) or periphery (orange box) of the cell ventral surface in (A).

(C) Internal and external views of stacked frames of ROI (dashed yellow box) in (B).

(D) Response of PIP3 wave to local EGF stimulation. Yellow star indicates the position of micropipette (applied at 0 min).

(E) Internal and external views of stacked frames of ROI (dashed yellow box) in (D).

(F) Wave maximum width versus distance to the micropipette in (D). The power regression is shown in dashed black line.

(G) Computational simulation of waves response to global stimulus based on an activator-inhibitor scheme. Green is activator (X) while red is inhibitor (Y). Global stimulus was added at time 0 (a.u.).

(H) Computational simulation of waves response to local stimulus. Green is activator while red is inhibitor. Yellow star indicates the position of stimulus.

4. A Small Decrease in PI(4,5)P2 Activates the Signal Transduction Network

PI(4,5)P2, as the substrate of the reaction, is reduced during the production of PI(3,4,5)P3 by activated Ras-PI3K network. We therefore tested how acute perturbations to PI(4,5)P2 reduction affect excitability in MCF-10A and MDA-MB-231 cells. To rapidly lower the level of PI(4,5)P2, we recruited the 5-phosphatase, Inp54p, using chemically induced dimerization (CID) (Figure 5A). Membrane recruitment of Inp54p caused an immediate reduction of PI(4,5)P2, detected by the translocation of the PI(4,5)P2-binding domain PH-PLCΔ, from the membrane to the cytoplasm (Figure 5B). Recruitment of a catalytically inactive mutant Inp54p (D281A) did not affect PH-PLCΔ localization (Figure 5C).

In MCF-10A cells, PI(4,5)P2 reduction triggered two distinct types of responses: spreading or retraction (Figure 6A). Spreading cells increased their basal surface area and showed ruffles, whereas retracting cells formed blebs around cell perimeter. We noticed that, compared to retracting cells, the spreading cells had lower expression levels of Inp54p (Figure 6B), suggesting that the type of response depends on the extent of PI(4,5)P2 reduction. To test this possibility, we observed individual cells exposed to increasing doses of rapamycin. Whereas a low dose (5 nM) rapamycin caused a slight increase in cytosolic PH-PLCΔ and strong cell spreading, a subsequent higher dose (1 μM) of rapamycin caused a further increase in cytosolic PH-PLCΔ which led to contraction (Figure 6C and 6D). Moreover, when cells were sorted according to the intensity of Inp54p fluorescence, most of the low or high expressers, respectively, spread or retracted (Figure 6E and 6F). Cells expressing a catalytically inactive Inp54p mutant did not respond to rapamycin addition (Figure 6F).

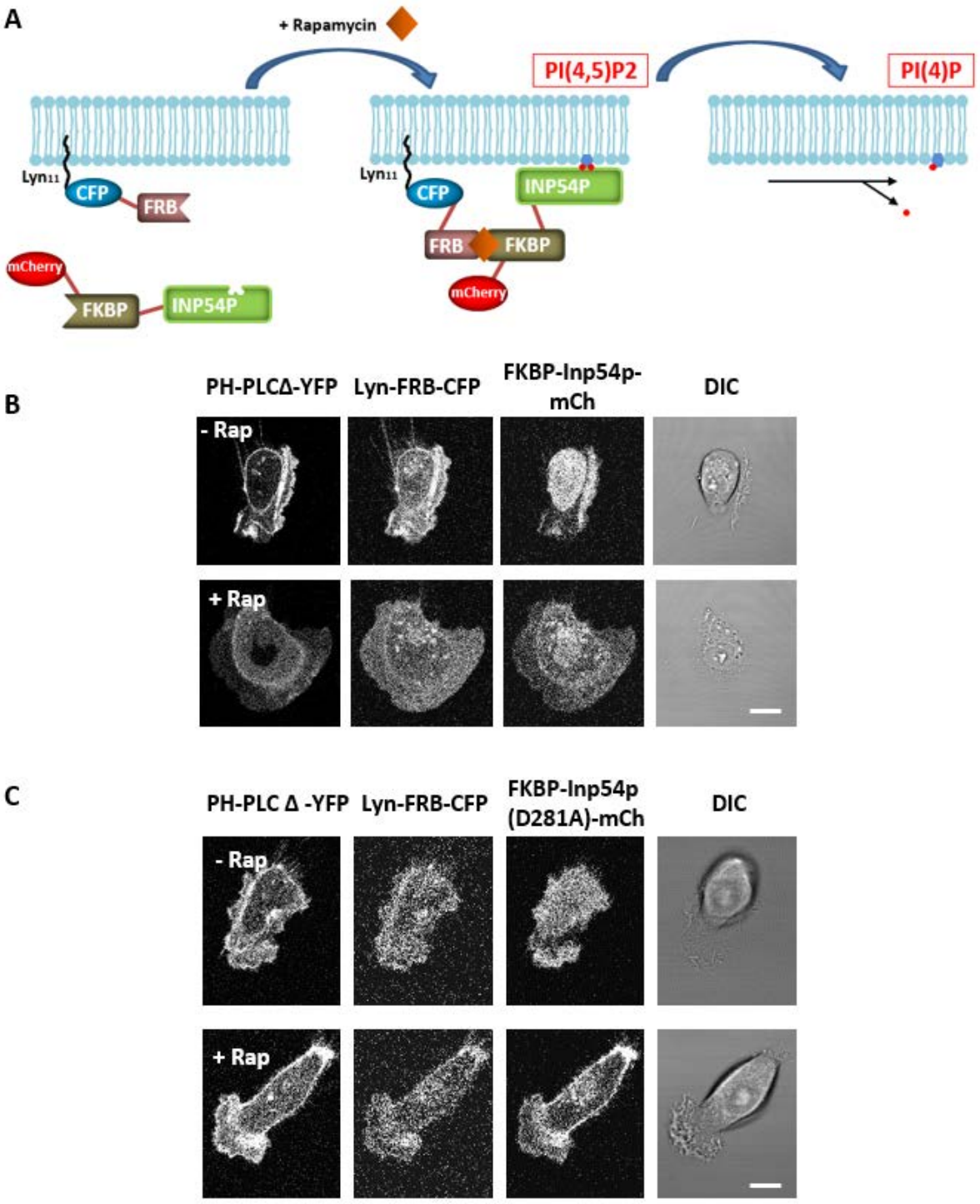

Figure 5. Recruitment of Inp54p by chemically-induced dimerization leads to rapid decrease in PI(4,5)P2.

(A and B) MCF-10A cells expressing Lyn-FRB, FKBP-Inp54p, and PH-PLCΔ were exposed to 1μM Rapamycin.

(Continued)

Images of single cell before and after the stimulation show diffusion of PH-PLCΔ from membrane to cytosol.

(C) The Inp54p inactive version (D281A) did not cause PI(4,5)P2 reduction.

The morphological changes induced by modest lowering of PI(4,5)P2 in MCF-10A cells were dynamic and associated with biochemical responses. Within minutes of addition of rapamycin, peripheral regions of the cell began to spread rhythmically (Figure 7A). Kymographs of the length of the lamellipodia revealed that the protrusions propagated around the perimeter with a period of about 20 min, suggesting they are driven by scroll waves (Figure 7B). The protrusions were labeled with RBD (biosensor for active Ras) (Figure 7C, 8A and 7D) and PH-AKT (Figure 8B), indicating locally elevated Ras and PI3K activity at protrusions drove the oscillatory spreading. The overall activity of Ras also increased when PI(4,5)P2 was lowered (Figure 7E and 7F). We therefore examined the downstream effectors of these activities. Immunofluorescence staining revealed a wide band of S473-AKT phosphorylation, indicating the activation of mTORC2 at the protrusions (Figure 8C). We also noticed that lowering of PI(4,5)P2 triggered ERK activation, detected by the nuclear exit of the biosensor ERK-KTR (Regot et al., 2014) (Figure 7G and 7H). The extent of ERK activation within the cell population was heterogeneous (Figure 7I). Furthermore, during continuous stimulation, the elevated steady-state level fluctuated (Figure 7H and 7I). Together the results indicate that PI(4,5)P2 lowering activates the Ras signaling network, which leads to activation of multiple downstream events. In MDA-MB-231 cells, slight PI(4,5)P2 lowering led to more PH-AKT and RBD waves in the interior regions of the basal cell surface and more ruffles at the cell edge. The increase in waves covering the basal surface was due to both *de novo* initiation as well as growth in pre-existing waves (Figure 7J-L). The temporal evolution of these waves is demonstrated by the t-stack of a section through the images (Figure 8D). Patches of PIP3 or RBD appeared in the interior upon rapamycin addition, indicating new wave formation. PIP3 or RBD enriched oscillatory protrusions also appeared on the perimeter. As in MCF-10A cells, slight

decrease of PI(4,5)P2 mostly caused spreading while large depletion of PI(4,5)P2 caused retraction and blebbing in MDA-MB-231 cells (Figure 8E).

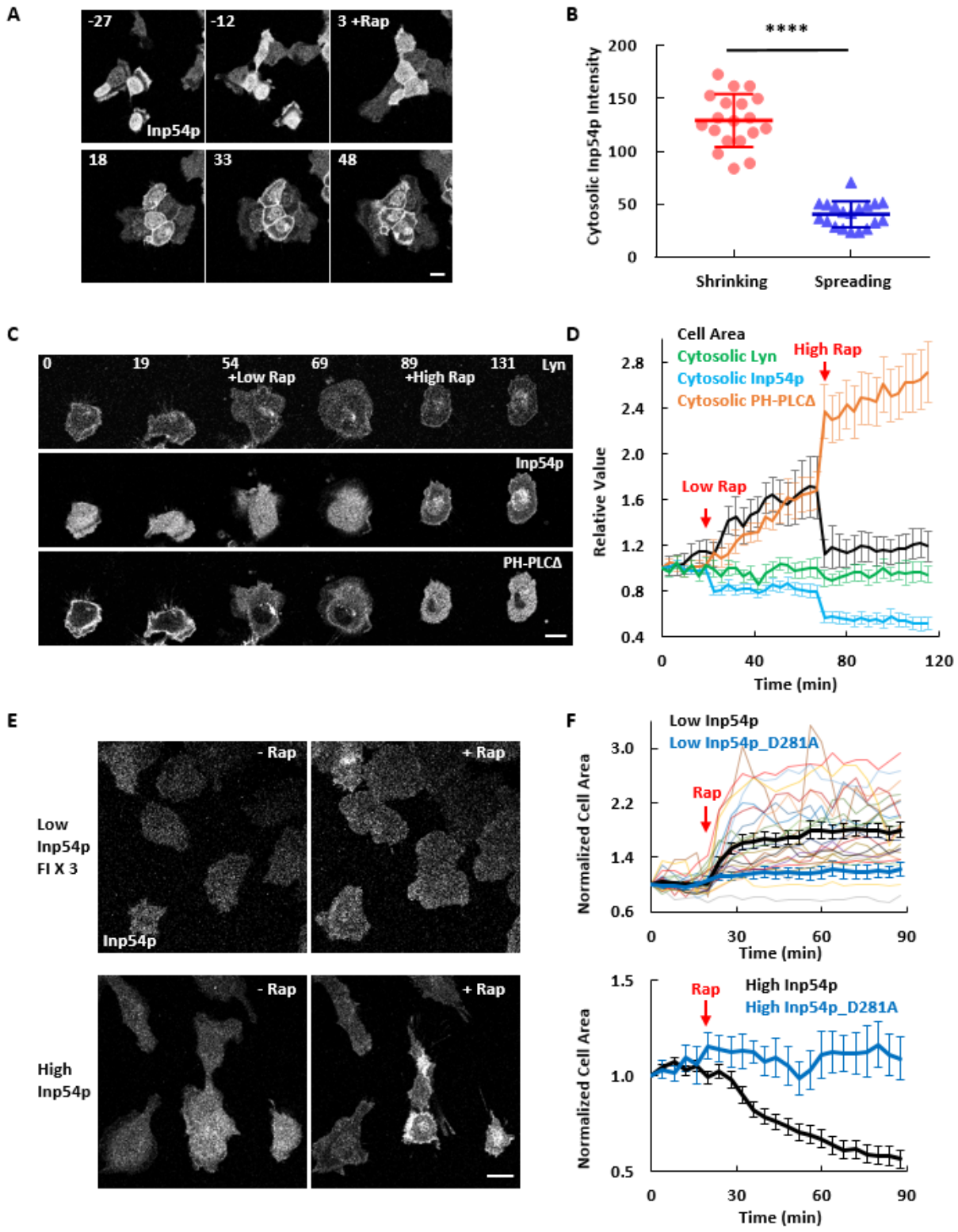

Figure 6. Low degree of PI(4,5)P2 reduction leads to cell spreading while high degree of PI(4,5)P2 reduction leads to cell shrinking.

(Continued)

(A) Response to 1μM rapamycin (added at 0 min) of a population of MCF-10A cells expressing Lyn-FRB and various levels of FKBP-Inp54p (channel shown).

(B) Quantification of cytosolic Inp54p intensity in shrinking or spreading cells. Cells with at least a 50% decrease in cell area are defined as shrinking while those with at least a 50% increase are defined as spreading (mean ± S.D. of n = 19 cells). Unpaired t test with Welch's correction, $p < 0.0001$.

(C) Different responses of single cell expressing Lyn-FRB, PH-PLCΔ, and high FKBP-Inp54p to low (5 nM) and subsequently high (1 μM) rapamycin at 20 and 70 min, respectively.

(D) Quantification of cell area and cytosolic intensity of PH-PLCΔ, FKBP-Inp54p, and Lyn-FRB in (C) (mean ± S.E.M. of n = 14 cells).

(E) MCF-10A cells were sorted into two groups (high Lyn-FRB/high FKBP-Inp54p and high Lyn-FRB/low FKBP-Inp54p) and cells responded uniformly in each group to 1μM rapamycin. The fluorescence intensity (FI) of low FKBP-Inp54p group was multiplied by 3.

(F) Quantification of cell area change in (E) (mean ± S.E.M. of n = 24 cells for low FKBP-Inp54p, 15 cells for low FKBP-Inp54p_D281A, 32 cells for high FKBP-Inp54p and 14 cells for high FKBP-Inp54p_D281A). The thin, colored lines represent the individual low Inp54p cells.

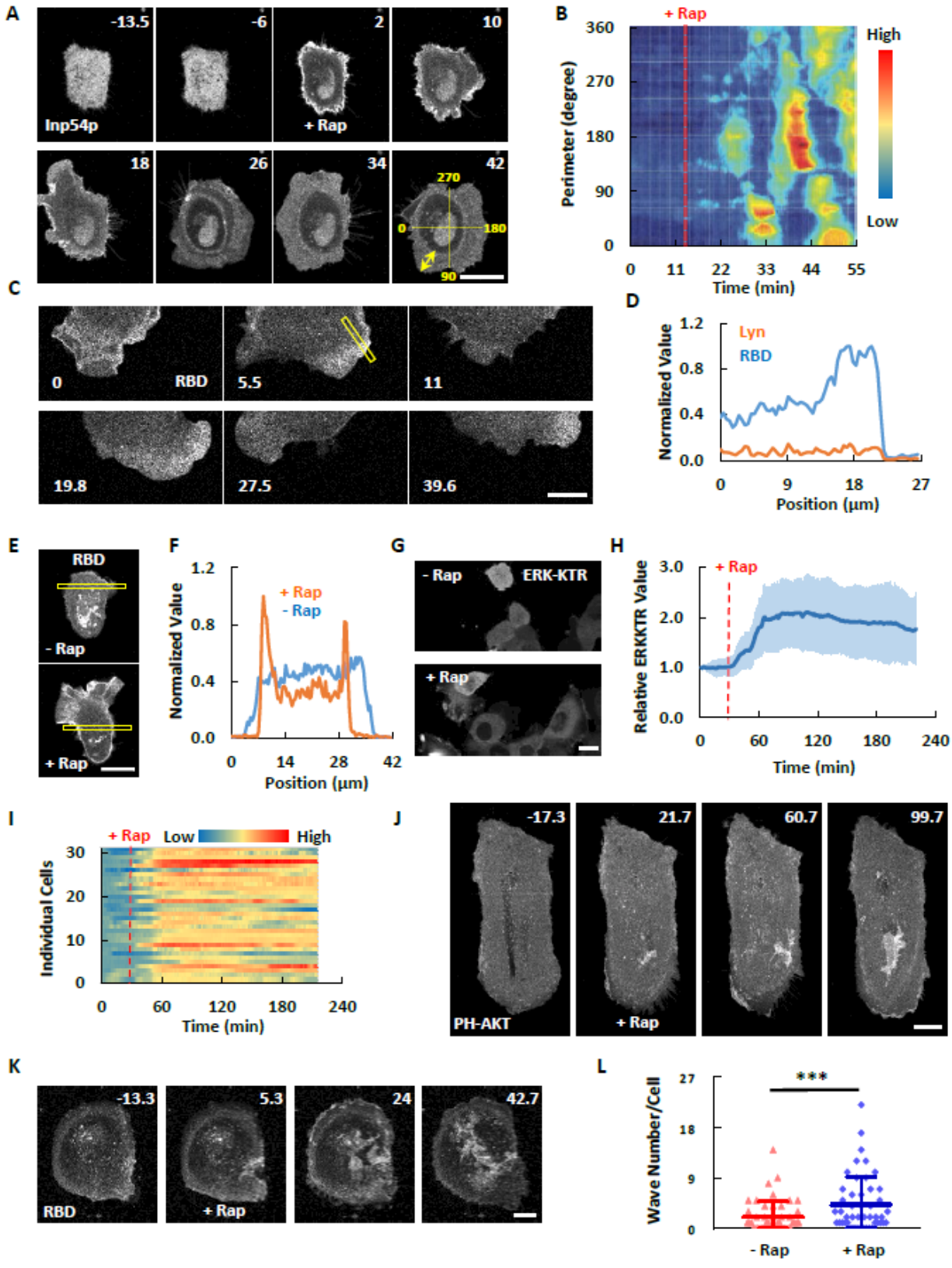

Figure 7. Morphological and signaling responses to PI(4,5)P2 reduction.

(Continued)

(A) Time-lapse confocal images of MCF-10A cell expressing Lyn-FRB and FKBP-Inp54p (channel shown). Rapamycin was added at 0 min.

(B) Kymograph of lamellipodia length around the perimeter of the cell in (A).

(C) Time-lapse confocal images of MCF-10A cell expressing Lyn-FRB (shown in Figure 8A), FKBP-Inp54p, and RBD (channel shown) after rapamycin indicate active Ras enriched at the oscillatory protrusions.

(D) Quantification of the boxes scan in (C) and Figure 8A.

(E) Confocal images of MCF-10A cell expressing Lyn-FRB, FKBP-Inp54p, and RBD (channel shown) before and after rapamycin.

(F) Quantification of the boxes scan in (E).

(G) Confocal images of MCF-10A cells expressing Lyn-FRB, FKBP-Inp54p, and ERK-KTR (channel shown) before and after rapamycin.

(H and I) Inverted nuclear intensity of ERK-KTR normalized to Lyn in population average (H, mean ± S.D. of n = 31 cells) and individual MCF-10A cells (I).

(J and K) Time-lapse confocal images showing increased PIP3 waves (J) or Ras waves (K) formation after lowering PI(4,5)P2 in MDA-MB-231 cells. Rapamycin was added at 0 min. T-stack analysis of (J) is presented in Figure 8D.

(L) Quantification of wave number change in (J and K). Individual waves were followed from origin to end in videos. The total wave number for each cell was quantified during 1 h imaging windows before and after rapamycin (mean ± S.D. of n = 48 cells, 5 experiments). Paired t test, p = 0.0004.

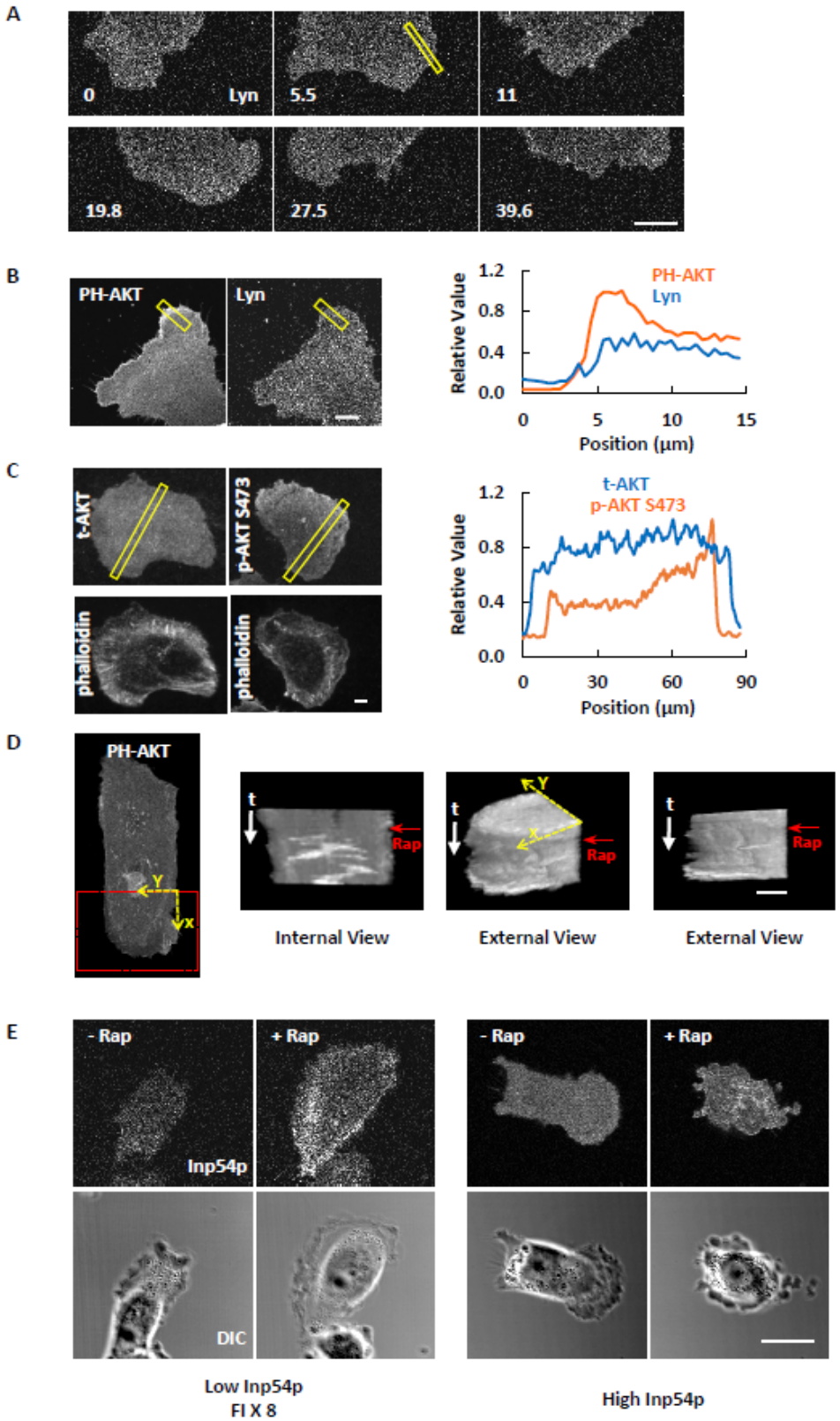

Figure 8. PI(4,5)P2 lowering activates PI(3,4,5)P3 and mTORC2.

(Continued)

(A) Lyn-FRB channel of cell in Figure 7C.

(B) Left panel: representative images of MCF-10A cell expressing Lyn-FRB (channel shown), FKBP-Inp54p, and PH-AKT (channel shown) after rapamycin. Right panel: quantification of the yellow boxes scan.

(C) Left panel: representative immunofluorescence staining images captured on TIRF of MCF-10A cell expressing Lyn-FRB and FKBP-Inp54p after rapamycin. Right panel: quantification of the yellow boxes scan.

(D) Internal and external views of stacked frames of ROI (dashed red box) of the cell in Figure 7J. The scale bar of time is 1 hour.

(E) MDA-MB-231 cells expressing Lyn-FRB, PH-AKT and different levels of FKBP-Inp54p (channel shown) before and after rapamycin. The fluorescence intensity (FI) of low FKBP-Inp54p cell was multiplied by 8.

5. A Small Decrease in PI(4,5)P2 Lowers the Threshold of the Excitable Network

Theoretically in excitable systems, the amount of spontaneous activity depends on the set point or threshold of the system. The generation of dynamic protrusions in MCF-10A cells and traveling waves in MDA-MB-231 cells suggested that PI(4,5)P2 lowering decreased the threshold of the excitable signaling network. To test this idea, we compared EGF-triggered ERK responses of MCF-10A cells in the presence or absence of PI(4,5)P2 lowering. PI(4,5)P2 lowering led to a greater percentage of cells responding to sub-saturating EGF stimulation (Figure 9A-E). When stimulated with increasing levels of EGF, the dose-response curve of PI(4,5)P2-reduced cells was left-shifted relative to that of the control cells (Figure 9F). Together these results suggested that slight PI(4,5)P2 reduction lowers the threshold of the excitable signaling network involving Ras, PI3K, and ERK.

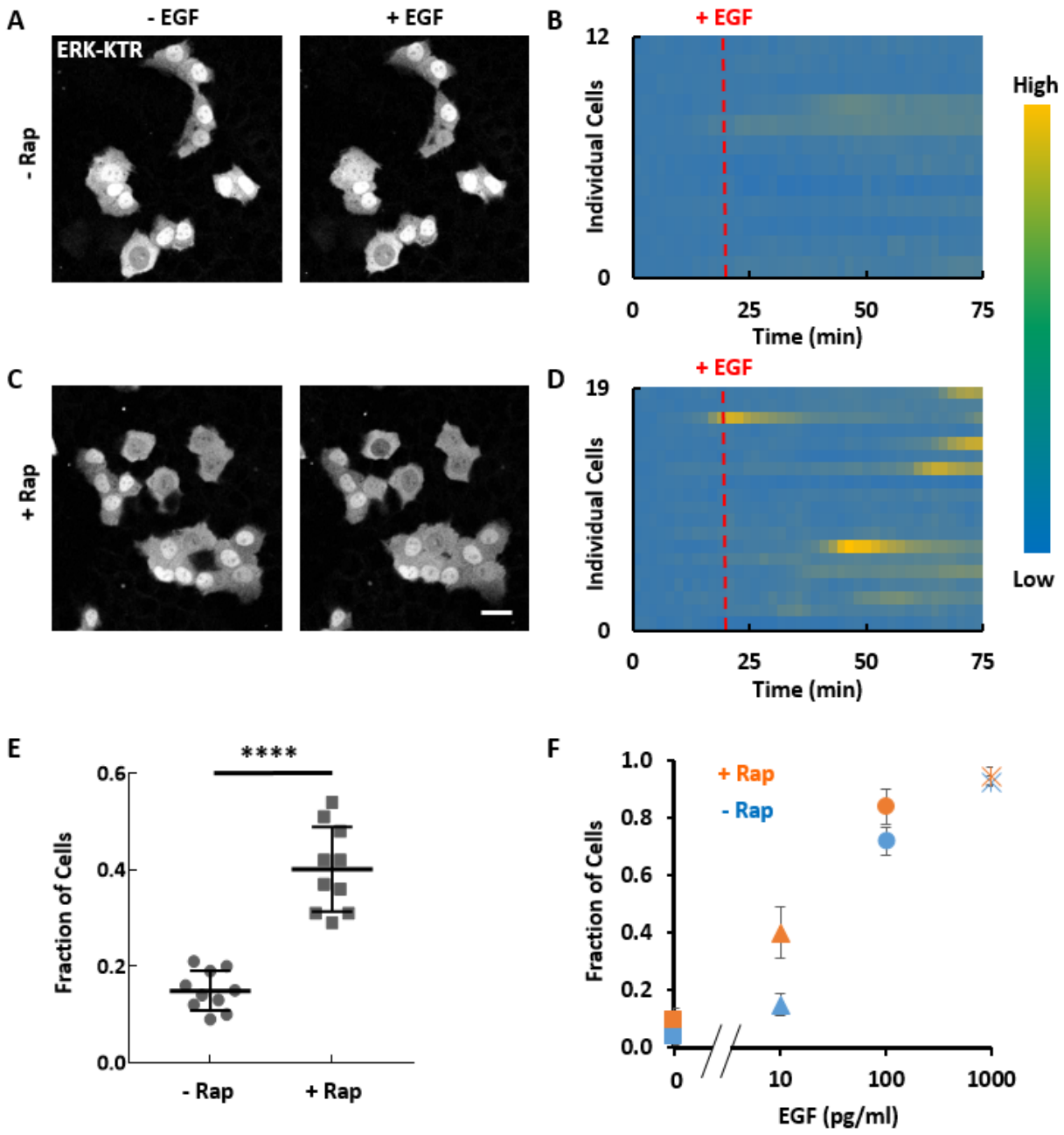

Figure 9. Effects of PI(4,5)P2 reduction on the threshold of ERK activation in MCF-10A cells.

(A-D) Responses of ERK-KTR to 10 pg/ml EGF stimulation in MCF-10A cells without (A and B) and with (C and D) PIP2 reduction by rapamycin-induced recruitment of Inp54p. Quantification of the inverted nuclear intensity of ERK-KTR (as Figure 7H) over time for 12 and 19 cells is shown in (B) and (D).

(Continued)

(E) Fraction of cells showing at least 50% increase in the inverted nuclear intensity of ERK-KTR (as Figure 7H) in response to 10 pg/ml EGF global stimulation without or with PIP2 reduction by rapamycin-induced recruitment of Inp54p (mean ± S.D. of n = 10 experiments). Unpaired t test with Welch's correction, $p < 0.0001$.

(F) Fraction of cells responding to global stimulation of various concentrations of EGF in cells without or with PIP2 reduction by rapamycin-induced recruitment of Inp54p (mean ± S.D. of n = 10 experiments).

6. mTORC2 Links Signal Transduction and Cytoskeletal Activities

To further define the mediators of the morphological changes induced by PI(4,5)P2 reduction, we blocked key pathways downstream of Ras using small molecule inhibitors. Although PI3K inhibitor LY294002 caused retraction of protrusions in unstimulated MCF-10A and MDA-MB-231 cells, the morphological changes induced by PI(4,5)P2 reduction still occurred in the presence of the inhibitor. However, when cells were treated with PP242, a dual mTORC1/2 inhibitor, S473-AKT phosphorylation was blocked (Figure 10A) and the PI(4,5)P2 lowering-induced cell spreading response was abolished (Figure 11A-C). Consistently, the response was also blocked by knocking down of mTOR with shRNA (Figure 10B, 11D, 11E and 11G). We do not believe that this effect is due to inhibition of mTORC1 since as noted above mTORC1 specific inhibitor rapamycin did not alter cell behavior. It was further confirmed by the result that shRictor also blocked the cell spreading response induced by decreasing PI(4,5)P2 (Figure 10C, 11D, 11F and 11G). Together these results suggested that mTORC2 mediates the effect of PI(4,5)P2 reduction on cytoskeletal activity.

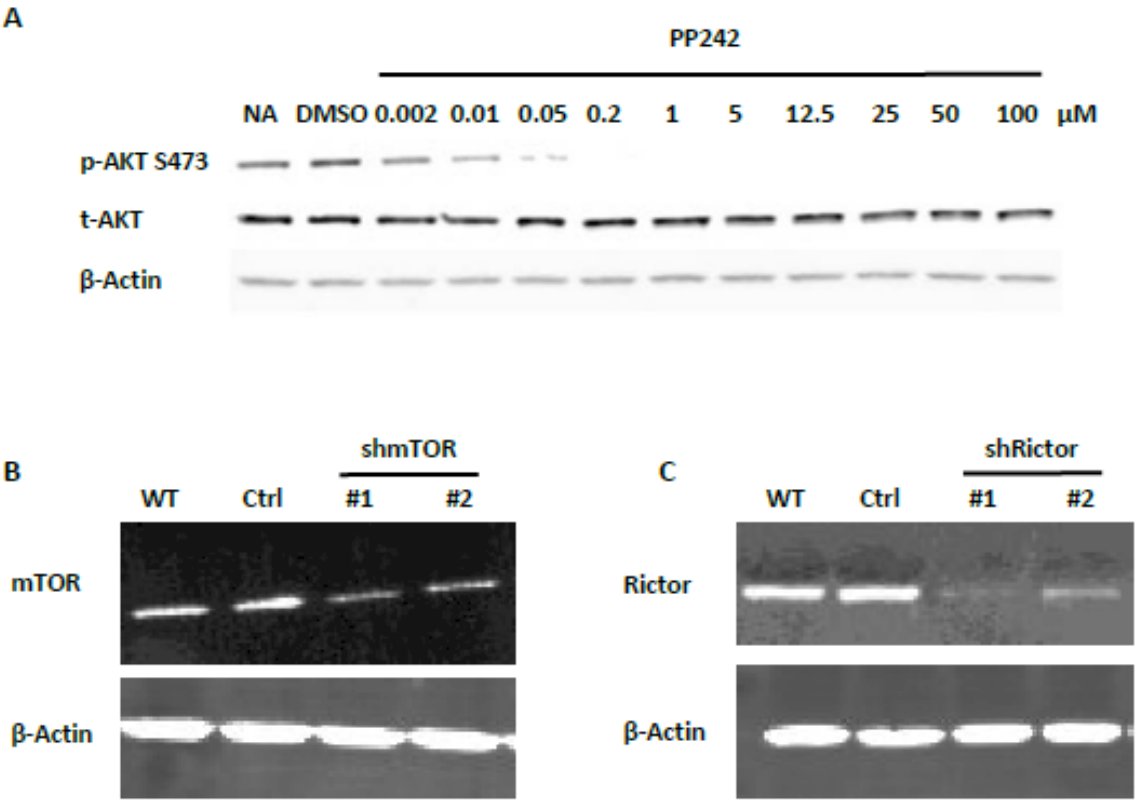

Figure 10. mTORC2 activity is inhibited by PP242 and mTOR or Rictor expression levels are lowered by shRNAs in MCF-10A cells.

(A) Western-blot indicated the activity of mTORC2 was inhibited by PP242.

(B and C) Western-blot indicated the expression levels of mTOR or Rictor were lowered by their shRNAs respectively. Control was the scrambled shRNA.

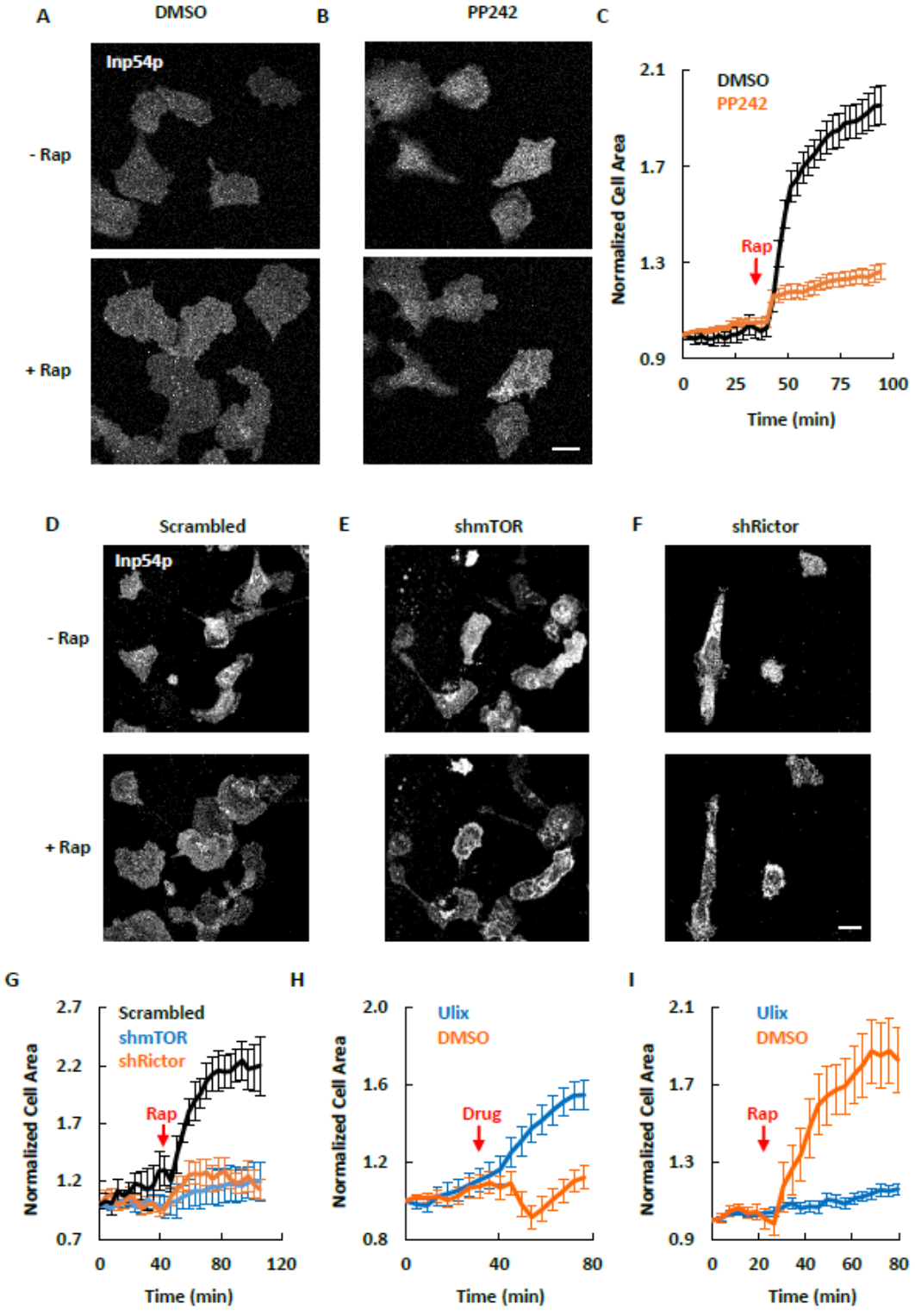

Figure 11. Morphological responses of MCF-10A cells to PI(4,5)P2 reduction depend on mTORC2 and ERK.

(Continued)

(A and B) Confocal images of MCF-10A cells expressing Lyn-FRB and FKBP-Inp54p (channel shown) pre-treated with DMSO (A) or 10 μM mTOR inhibitor PP242 (B) before and after rapamycin.

(C) Quantification of area changes of cells in (A and B) (mean ± S.E.M. of n = 15 cells).

(D-F) Confocal images of MCF-10A cells expressing Lyn-FRB and FKBP-Inp54p (channel shown) transfected with scrambled (D), mTOR (E), or Rictor (F) shRNAs before and after rapamycin.

(G) Quantification of area changes of cells in (D-F) (mean ± S.E.M. of n = 20 cells).

(H) Quantification of area changes of MCF-10A cells treated with DMSO or 10 μM Ulixertinib (ERK inhibitor) (mean ± S.E.M. of n = 20 cells for Ulix and 22 for DMSO).

(I) Quantification of area changes of MCF-10A cells before and after rapamycin-induced PIP2 reduction (mean ± S.E.M. of N = 18 cells for Ulix and 17 for DMSO). Cells were either pre-treated with DMSO or 10 μM Ulixertinib for 2h before the addition of rapamycin.

7. Cytoskeletal Activity is Not Required for the PI(4,5)P2 Lowering Mediated Signaling Activation

We wonder whether the cytoskeletal activity is required for the PI(4,5)P2 lowering mediated signaling activation. To arrest cytoskeletal dynamics and maintain cell shape (Peng et al., 2011), we used a pharmacological cocktail (JLY): a total of 10 μM Y27632 was added to MDA-MB-231 cells, and 5 μM Latrunculin B and 8 μM Jasplakinolide were added 10 min later. Subsequently addition of rapamycin to introduce the lowering of PI(4,5)P2 still caused the significantly increased formation of PI(3,4,5)3 at the perimeter of MDA-MB-231 cells (Figure 12). This suggests that the PI(4,5)P2 lowering mediated signaling activation does not require the involvement of cytoskeletal activity.

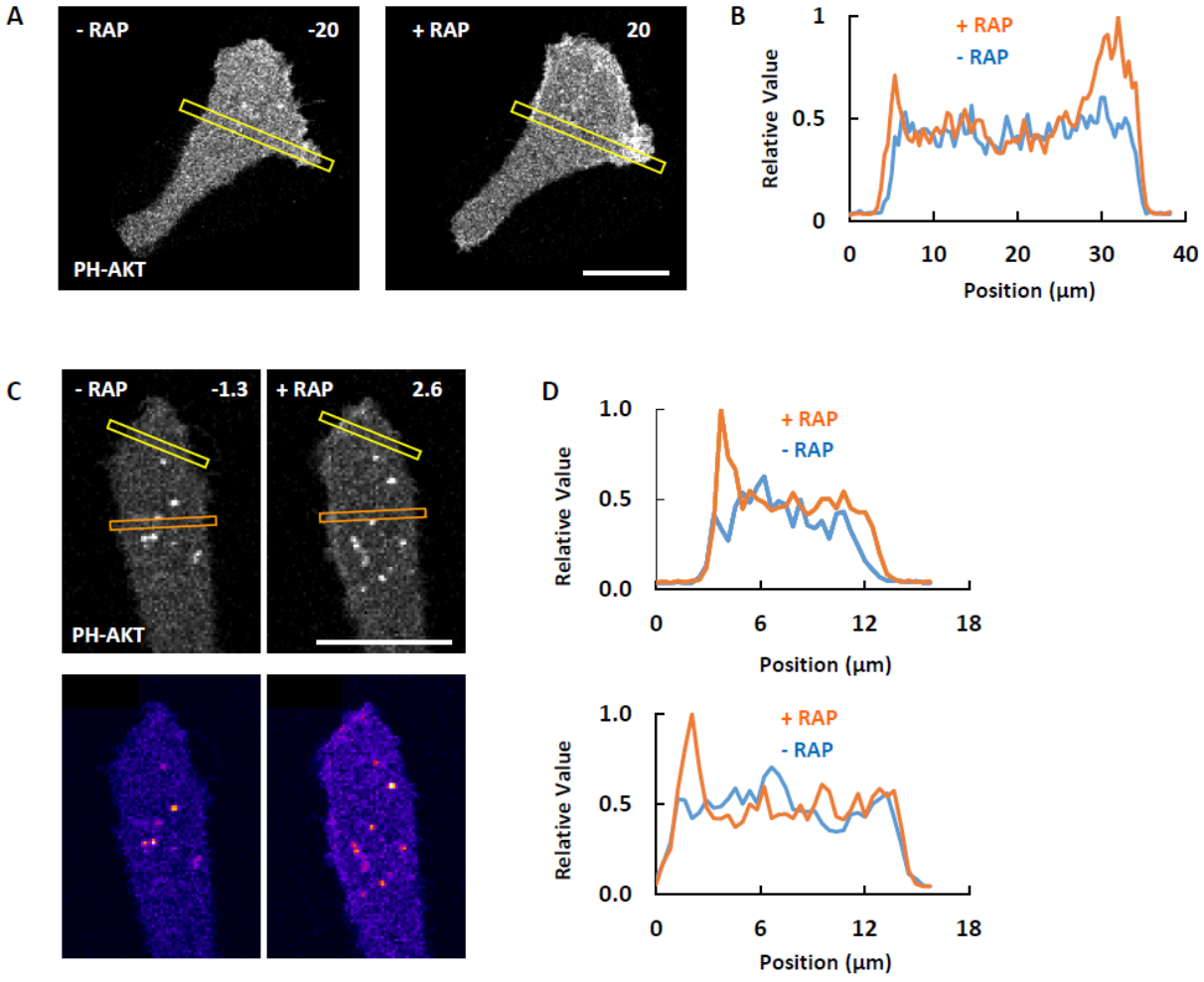

Figure 12. PIP3 production was activated after PI(4,5)P2 lowered with the inhibition of cytoskeletal activity.

(A) MDA-MB-231 Cell was expressed with Lyn-FRB, INP54P-FKBP, and PH-AKT (channel showed). Cell was pretreated with JLY (referred to the main text for experimental details) 1 hour before imaging. 1 μM rapamycin was added at 0 min.

(B) Quantification of the yellow boxes scan in (A).

(Continued)

(C) Experimental setting was same to (A). Upper panel are the gray-scale confocal images, while lower panel are the corresponding fire-scale images.

(D) Upper graph is the quantification of the yellow boxes scan in (C), and lower graph is the quantification of the orange boxes scan in (C).

8. ERK and PI(3,4)P2 are Negative Regulators in the Excitable Network

Since ERK is activated by PI(4,5)P2 lowering (Figure 7G-I), we tested the role of ERK in mediating the spreading response. Surprisingly the ERK inhibitor Ulixertinib alone caused more cell spreading but not to the same extent as PI(4,5)P2 lowering (Figure 11H). Subsequent lowering of PI(4,5)P2 after ERK inhibition caused no further increase in cell spreading (Figure 11I). This suggests that major role of ERK is a negative regulator of the system.

Recent evidence suggests that PI(3,4)P2 has physiological roles in addition to being a product of PI(3,4,5)P3 degradation (Gewinner et al., 2009; Hawkins et al., 2016; Guo et al., 2016; Malek et al., 2017; Goulden et al., 2019). We compared the dynamic levels of PIP3 and PI(3,4)P2 using biosensors PH-AKT and PH-TAPP1. While PIP3 and PI(3,4)P2 both localized on cell protrusions, they were spatially separated. PIP3 formed a band at the perimeter and PI(3,4)P2 formed a trailing band back from the perimeter in both MDA-MB-231 and MCF-10A cells (Figure 13A-C).

We next measured the kinetics of PIP3 and PI(3,4)P2 changes in response to EGF in MCF-10A cells. Upon stimulation, PIP3 and PI(3,4)P2 increased globally on the membrane. PIP3 reached a peak within 2 min, while PI(3,4)P2 rose more slowly and peaked 1 min later (Figure 13D). The difference in the kinetics is consistent with the spatial relationship seen in propagating waves and protrusions.

To determine the role of PI(3,4)P2 in the excitable network, we assessed the effects of acute reduction of PI(3,4)P2. We used CID to recruit INPP4B to hydrolyze PI(3,4)P2. Upon the addition of rapamycin, MCF-10A cells begin to carry out oscillatory spreading, consistent with an increase in wave activity (Figure 13E, 13F and 14). This contrasted strikingly to the effects of PIP3

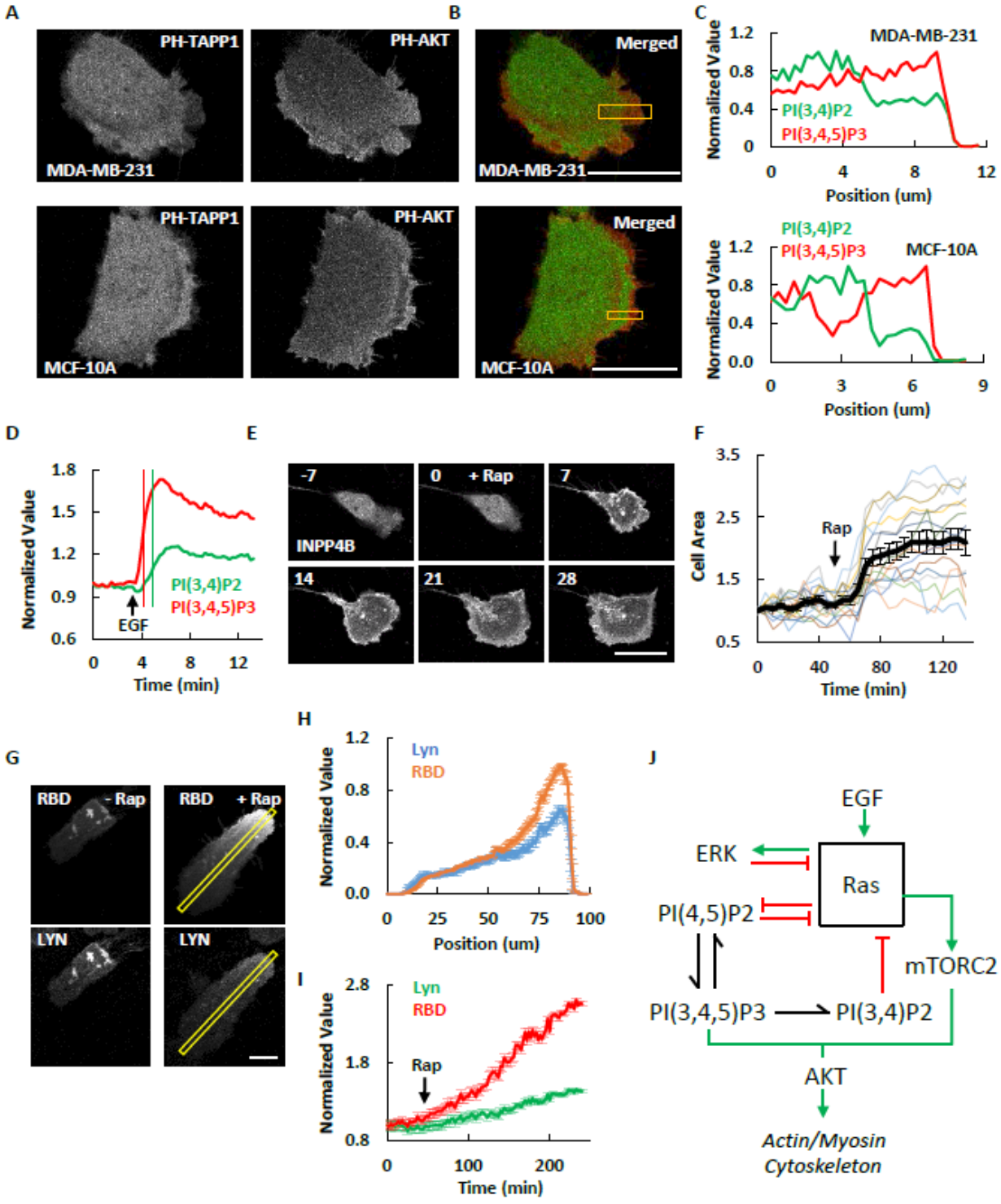

Figure 13. PI(3,4)P2 is a negative regulator of the excitable network.

(A) Confocal images of MDA-MB-231 or MCF-10A cells expressing PH-TAPP1-GFP and PH-AKT-RFP.

(Continued)

(B) Merged images of both fluorescence channels in (A). Green is PH-TAPP1 and red is PH-AKT.

(C) Quantification of the boxes scan in (B).

(D) PI(3,4)P2 and PI(3,4,5)P3 responses to global EGF stimulation in MCF-10A cell. Thin vertical lines mark 50% values.

(E) Time-lapse confocal images of MCF-10A cell expressing Lyn-FRB and FKBP-INPP4B (channel shown). Rapamycin was added at 0 min.

(F) Quantification of the cell area changes of individual MCF-10A cells (colored lines) or population average (black line, mean ± S.E.M. of n = 15 cells) before and after rapamycin-induced PI(3,4)P2 reduction. The phosphatase inactive control is shown in Figure 12.

(G) Confocal images of the ventral surface of MCF-10A cell expressing Lyn-FRB (channel shown), FKBP-INPP4B, and RBD (channel shown) before and after rapamycin.

(H) Quantification of the yellow boxes scan in (G) (mean ± S.D. of n = 5 frames).

(I) Quantification of changes of RBD (red line) and Lyn (green line) at the ventral surface of MCF-10A cells before and after rapamycin-induced PI(3,4)P2 reduction (mean ± S.E.M. of n = 11 cells).

(J) Diagram of the working model. Green arrows indicate activating interactions while red bars indicate inhibitory interactions.

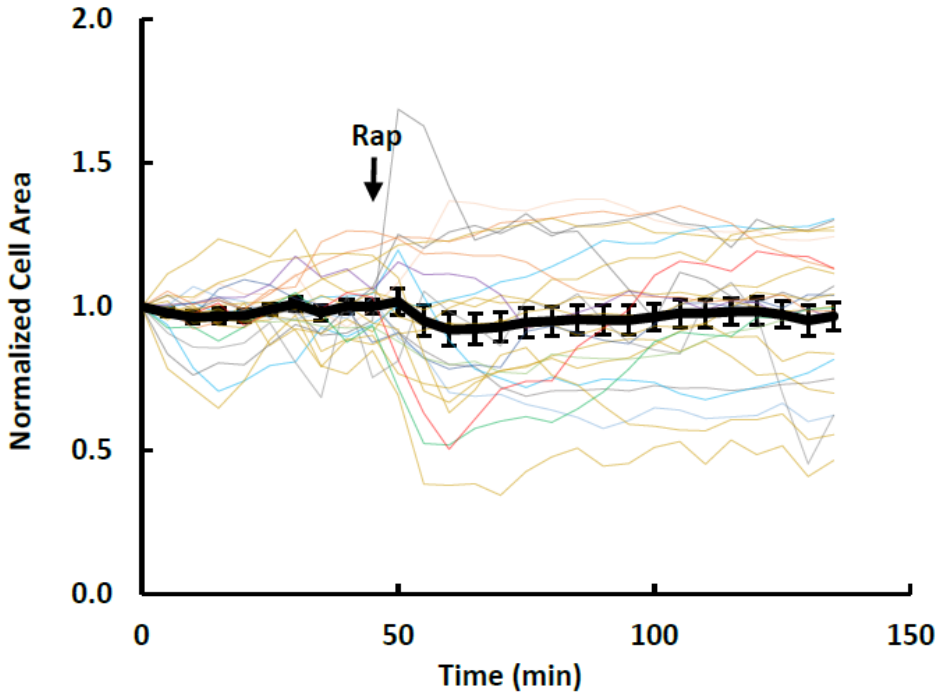

Figure 14. The recruitment of inactive INPP4B does not increase the spreading in MCF-10A cells.

Quantification of the area changes of individual cells (colored lines) or population average (black line, mean ± S.E.M. of n = 24 cells) before and after rapamycin. Cells were expressed with Lyn-FRB and FKBP-INPP4B(C842A) (an inactive form).

depletion which caused cell retraction. Furthermore, the morphological changes caused by PI(3,4)P2 reduction were accompanied by Ras activation as detected by its biosensor RBD (Figure 13G-I).

9. Oncogenic Transformation Causes Enhanced Excitability of the Signal Transduction Network

We examined the effect of Ras activation on network excitability and cell morphology. If the network outlined in Figure 13J is correct, an increase in Ras activity would be expected to lower the threshold and lead to increased excitability. To acutely activate Ras, we used chemically induced dimerization (CID) to rapidly recruit the CAAX-deleted constitutively active Kras_G12V to membrane-anchored Lyn-FRB upon rapamycin addition. In MCF-10A cells, Kras_G12V recruitment led to oscillatory cell spreading, similar to the effects of PI(4,5)P2 reduction (Figure 15A). The effects of recruiting Ras-GEF, CDC25, were similar to those induced by Kras_G12V (Figure 15B). In order to examine the effect of Ras activation on existing wave activities, we recruited CDC25 in MDA-MB-231 cells. As indicated by the PIP3 biosensor PH-AKT, activation of Ras led to an increase in the number of travelling waves on the basal surface of the cells (Figure 15C). As we have shown earlier, these changes are indicative of a lowered threshold of the signal transduction excitable network.

To directly correlate the excitability of the signaling network with cell oncogenic transformation, we examined MCF-10A cells expressing Hras, Kras or C-MYC oncogenes. These cells have been shown to display features of cell transformation including growth on soft agar (Basolo et al., 1991), epithelial to mesenchymal transition (Liu et al., 2009), and tumor formation in mouse xenografts (Imbalzano et al., 2009). In our hands, similar to PI(4,5)P2 lowering, the transformed cells were larger and more spread and showed lower resistance to hypotonic shock (Figure 16). Expression of LifeAct and PH-AKT revealed travelling actin and PIP3 waves moving across the basal surface as seen in MDA-MB-231 cells (Figure 15D-F). As noted earlier, basal waves within the cell perimeter were rarely detected in the control MCF-10A cells (Figure 15D). Transformed cells

displayed a variety of concentric or spiral waves as well as intermittent standing/traveling waves. Some waves initiated at the perimeter with one side of the wave propagating inward and the other pushing the cell edge outwards. Other waves started interiorly, traveled to the edge, and pushed out. In four experiments, 41.8 ± 5.9 % (mean ± SEM) of transformed cells and 5.9 ± 1.5 % (mean ± SEM) of control cells displayed these internal waves (Figure 15G). The transformed cell population had more spread cells than control MCF-10A cells; however, both small and large transformed cells displayed more waves and there was only a moderate correlation with cell size ($R^2 = 0.4443$) (Figure 17A and 17B). Furthermore, compared to control, spontaneous ERK activity increased and showed more frequent oscillations in Ras_G12V transformed cells (Figure 15 H-K). Since the increase in wave activity suggested that the threshold of the network is lowered, we examined the response of ERK to EGF stimulation of different doses in control and Kras_G12V cells. As shown in Figure 17C, the baseline activity of ERK was higher and the EC50 concentration of EGF needed to trigger responses was lower in the transformed cells. These results are consistent with the lowering of the threshold of signal transduction excitable network in PI(4,5)P2-reduced cells.

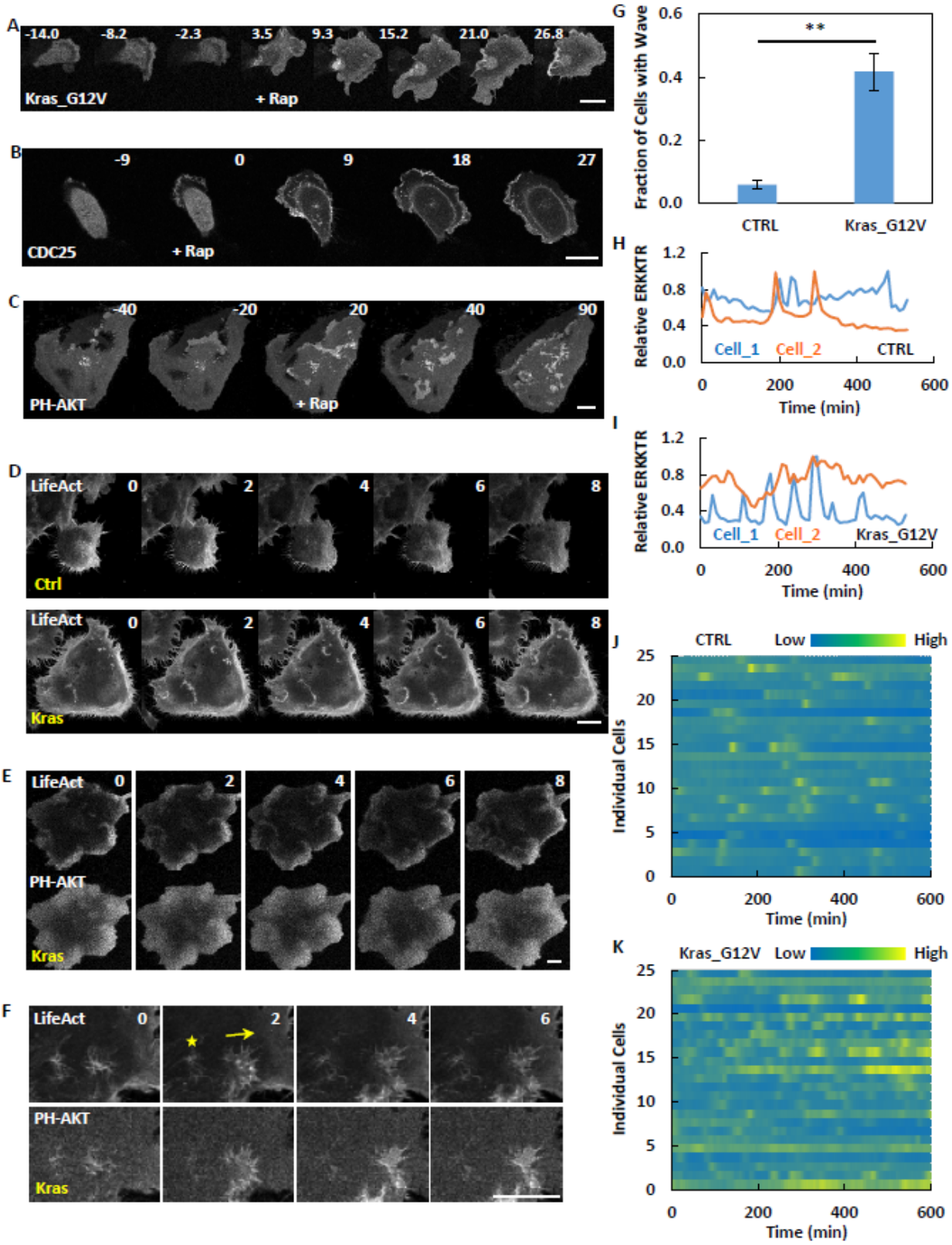

Figure 15. Oncogenic transformation causes enhanced excitability of the signal transduction network.

(Continued)

(A) Time-lapse confocal images of MCF-10A cell expressing Lyn-FRB and FKBP-Kras_G12V (channel shown). Rapamycin was added at 0 min.

(B) Time-lapse confocal images of MCF-10A cell expressing Lyn-FRB and FKBP-CDC25 (channel shown). Rapamycin was added at 0 min.

(C) Time-lapse confocal images of MDA-MB-231 cell expressing Lyn-FRB, FKBP-CDC25, and PH-AKT (channel shown). Rapamycin was added at 0 min.

(D) Time-lapse confocal images of control or Kras_G12V transformed MCF-10A cells expressing LifeAct (channel shown).

(E) Time-lapse confocal images of Kras_G12V transformed MCF-10A cell expressing LifeAct and PH-AKT (both channels shown).

(F) Time-lapse confocal images of Kras_G12V transformed MCF-10A cell expressing LifeAct and PH-AKT (both channels shown). Star indicates standing wave and arrow indicates traveling wave.

(G) Quantification of fraction of cells with wave in control or Kras_G12V transformed MCF-10A cells during a 2-hour imaging window (mean ± S.E.M. of n = 4 experiments, 306 control cells and 347 Kras transformed cells). Unpaired t test with Welch's correction, $p = 0.0071$.

(H and I) Inverted nuclear intensity of ERK-KTR (as Figure 7H) in two individual control (H) or Kras_G12V transformed (I) MCF-10A cells.

(J and K) Heat map of inverted nuclear intensity of ERK-KTR (as Figure 7H) of control (J) or Kras_G12V transformed (K) MCF-10A cells. n = 25 cells for each group.

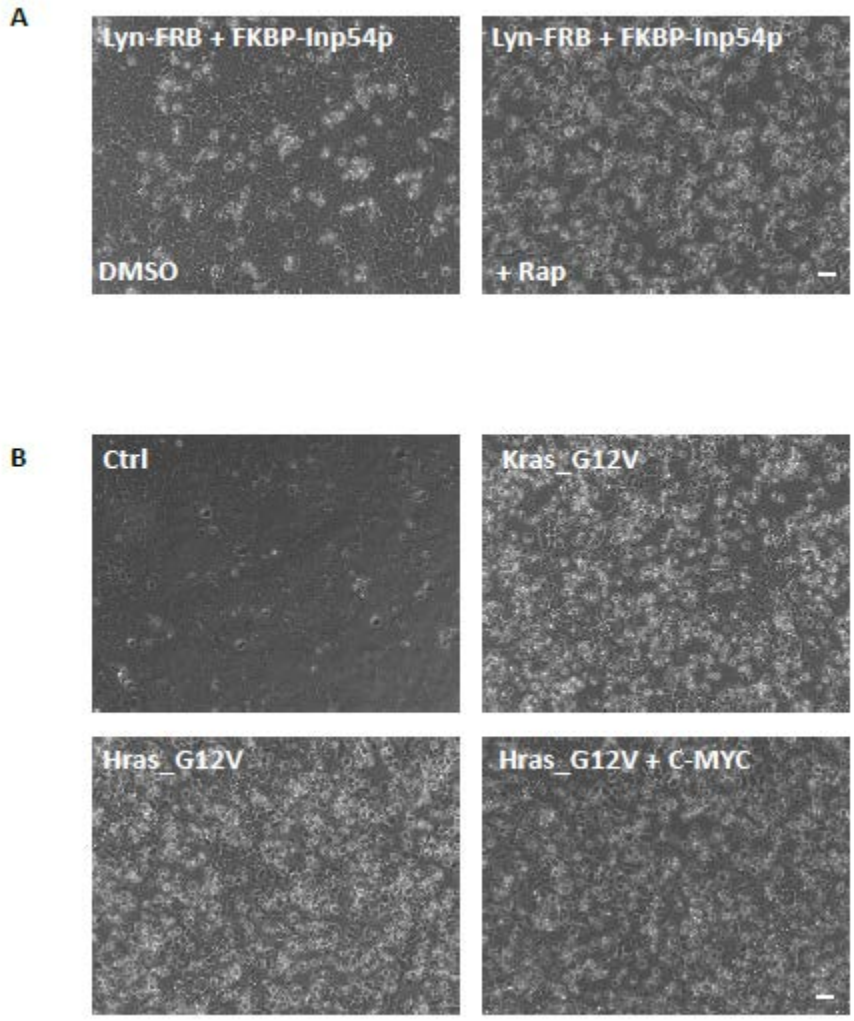

Figure 16. Hypotonic shock induces more cell death in PI(4,5)P2 lowered and Ras or/and C-MYC transformed MCF-10A cells.

(A) DIC images showed more cell death with PI(4,5)P2 lowered when given hypotonic shock. For hypotonic shock, MCF-10A cells were incubated in 1 volume hypotonic buffer (ddH2O + 1 mM MgCl2 + 1.2 mM CaCl2) : 4 volume growth media for 24 hours before imaging. DMSO or 1 μM rapamycin were given 2 hours before hypotonic shock.

(B) DIC images showed hypotonic shock caused more cell death in Ras_G12V or/and C-MYC transformed MCF-10A cells.

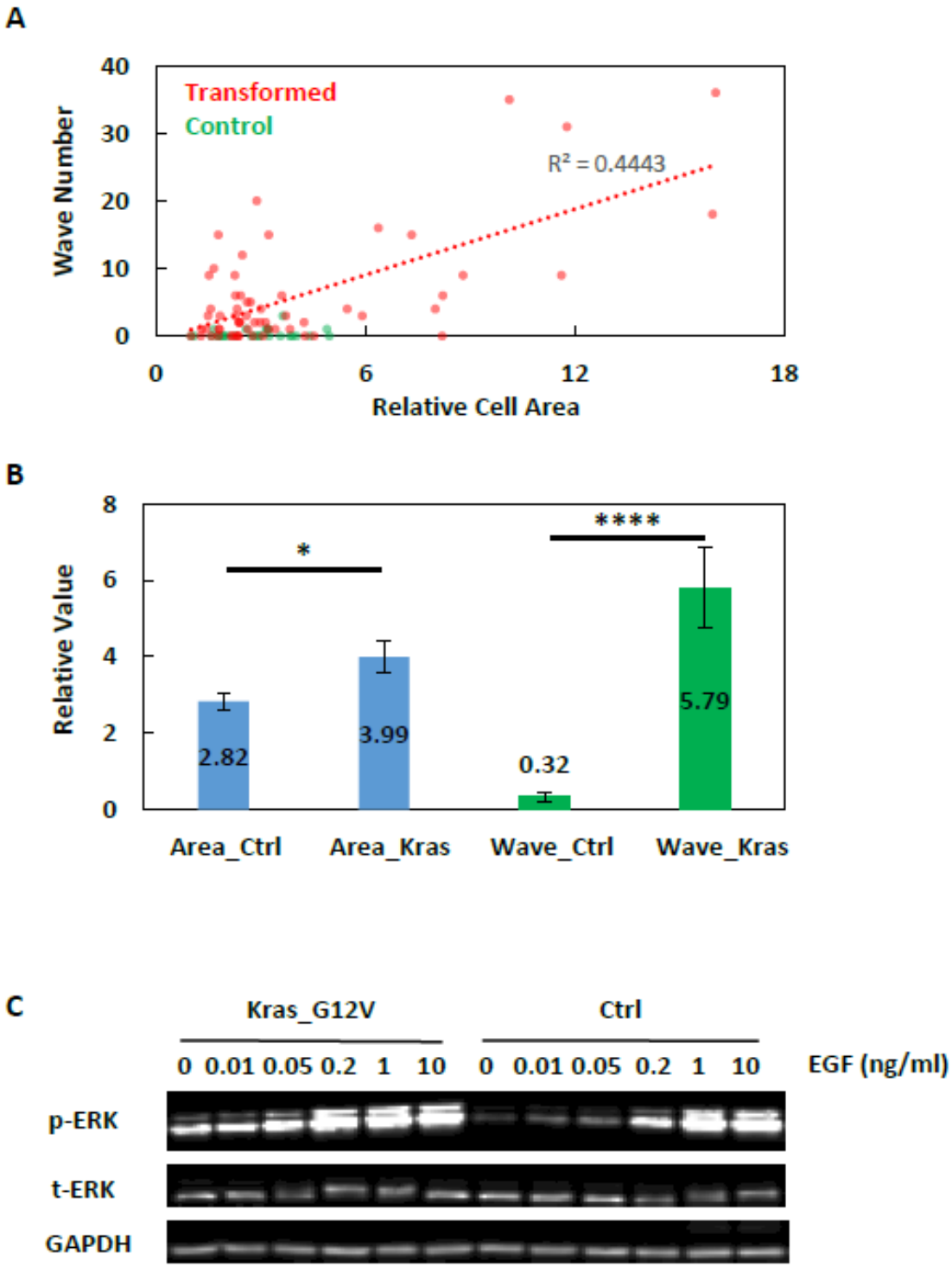

Figure 17. Kras_G12V transformed MCF-10A cells have increased wave number and cell area, and stronger ERK responses to EGF stimulation.

(Continued)

(A) Wave number (y-axis) in each individual cell was plotted by cell area (x-axis) during a 2-hour imaging window of control (green circles) and Kras_G12V transformed (pink circles) MCF-10A cells (n = 28 control and 61 transformed cells). The linear regression line is shown for transformed cells.

(B) Quantification of cell area and wave number per cell in control and Kras_G12V transformed MCF-10A cells (mean ± S.E.M. of n = 28 control and 61 transformed cells). Unpaired t test with Welch's correction, $p = 0.0166$ for area and < 0.0001 for wave number.

(C) Western Blot to show the shifted dose response of ERK to EGF stimulation in Kras_G12V transformed MCF-10A cells.

10. Increasing the Threshold of the Excitable Ras/PI3K/ERK Network Impairs the Wave and Protrusion Formation of Cancer Cells

The cancer transformation led to lower threshold of the excitable networks involving Ras, PI3K and ERK. We next asked what an increasing of threshold can do to a cancer cell. As indicated in Figure 13J, it is likely to increase the threshold of the signaling system by inhibiting the PIP3 production or mTORC2 activity. There was a dramatic overall decrease of PIP3 production at the ventral surface of a migrating breast cancer cell MDA-MB-231 (Figure 18A, 18C, and 18D) shortly after the addition of PI3K inhibitor ZSTK474. The significant decrease in numbers of propagating waves indicated that the threshold of the excitable network was increased (Figure 18B). This impaired the protrusion formation and led to shrinkage of cell size (Figure 18E). Similar effect was observed for PP242 treatment (Figure 19). Thus, increasing the threshold of the excitable network impairs the cancer cell migration.

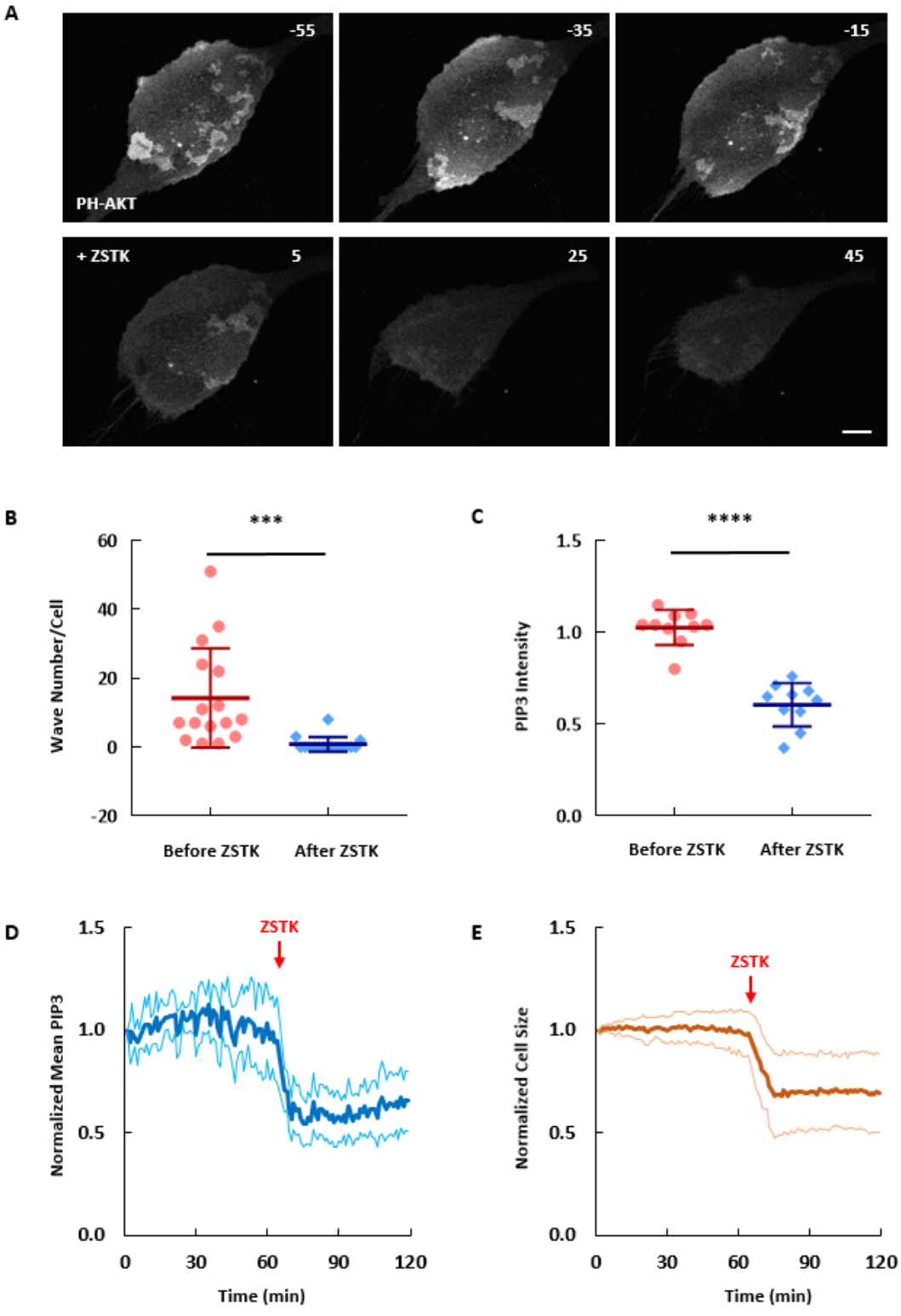

Figure 18. PIP3 depletion abolishes the propagating wave and reduces the cell size in MDA-MB-231 cancer cells.

(Continued)

(A) Time-lapse confocal images of MDA-MB-231 cell expressing PH-AKT to show the signaling of PIP3 at the bottom surface of the living cell. 10 μM PI3K inhibitor ZSTK was added at 0 min.

(B) Quantification of wave number change in (A). Individual waves were followed from origin to end in videos. The total wave number for each cell was quantified during 55 min imaging windows before and after ZSTK (mean ± S.D. of N = 16 cells). Paired t test, P = 0.001.

(C) Quantification of mean PIP3 intensity at the ventral surface of cells in (A). The PIP3 value on the left column is the average of all frames before the addition of ZSTK during the 65 min imaging window, while the PIP3 value on the right column is the average of all frames after the addition of ZSTK during the following 55 min imaging window. Paired t test, $P < 0.0001$.

(D) Quantification of the dynamic change of the mean PIP3 intensity at the ventral surface of cells in (A). ZSTK was added at 65 min. The bold dark blue line is the average while the two light blue lines are the mean ± S.D. of N = 10 cells.

(E) Quantification of the dynamic change of the size of cells in (A). ZSTK was added at 65 min. The bold dark orange line is the average while the two light orange lines are the mean ± S.D. of N = 10 cells.

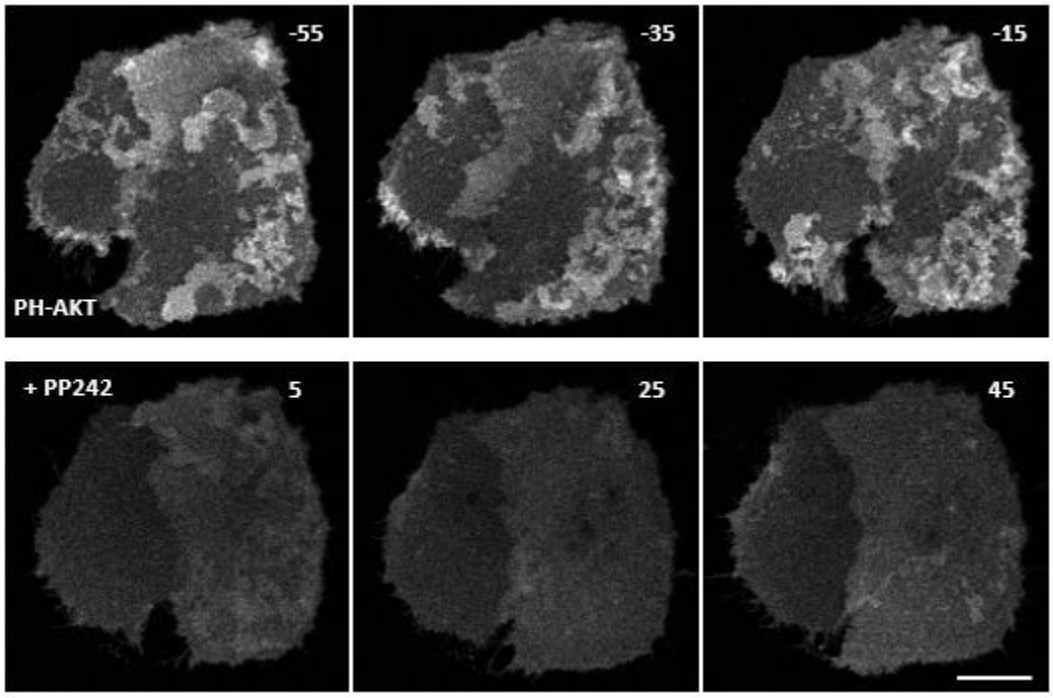

Figure 19. PP242 reduces the wave activity in cancer cells.

Time-lapse confocal images of MDA-MB-231 cell expressing PH-AKT to show the signaling of PIP3 at the bottom surface of the living cell. 10 μM mTOR inhibitor PP242 was added at 0 min.

Discussion

1. Summary

Our studies provide systems-level mechanisms for migratory transitions and oncogenic transformation in human epithelial cells. We found that, first, these cells display propagating waves of Ras and PI3K activation and that waves reaching the cell perimeter drive protrusions. External stimulation with growth factors can influence the wave behavior. Second, oppositely directed waves merge and display mutual annihilation and responses to growth factor display all-or-none responsiveness and refractory periods. Third, abrupt perturbations of Ras activity and phosphoinositide levels change the number and character of traveling waves and protrusions as well as the sensitivity to growth factor stimulation. These observations show that cellular protrusions are controlled by an excitable Ras/PI3K/ERK network and that growth factors guide cells by locally altering excitability. They also delineate the feedback loops that contribute to excitability. Finally, we discovered that Ras transformation leads to *de novo* or increased wave activity, consistent with the increased protrusive activity displayed by transformed cells.

2. Excitability of Ras/PI3K/ERK Network in Human Epithelial Cells

Multiple different criteria demonstrated that the Ras/PI3K/ERK network in human epithelial cells is excitable. There was no response to 30 sec growth factor stimulation while the responses to 1 min and 5 min were quite similar. The responses to 1 and 5 min stimuli continued to increase after the stimuli were removed, suggesting that the system responds in an all-or-none fashion after

crossing a threshold. A recent study suggested that EGFR activity is required for an all-or-none ERK response (Sparta et al., 2015). Paired stimuli demonstrated the existence of refractory period; cells required about 30 min to regain full responsiveness. The refractory period explains why oppositely directed waves annihilate and the duration of the refractory period is consistent with the period of ERK oscillations previously described in MCF-10A cell (Albeck et al., 2013).

3. Conservation from *Dictyostelium* to Human Epithelial Cells

The studies presented here show that actin waves in epithelial cells are regulated by a mechanism similar to that delineated in *Dictyostelium* (Vicker et al., 2002; Gerisch et al., 2004; Wozniak et al., 2005; Miao et al., 2017). In *Dictyostelium*, the slower kinetics of the signal transduction network lead to broad bands of Rap, Ras, and PI3K activity that move coordinately with leading and trailing peaks of F-actin polymerization/depolymerization. This behavior was attributed to the coupling of a slow signal transduction excitable network (STEN) to a rapid cytoskeletal excitable network (CEN). These characteristics are apparently conserved in human epithelial cells reported here. We found previously reported actin "rosettes" (Marchesin et al., 2015) consisted of a narrow actin band accompanied by broader bands of Ras activation and PIP3. The duration of the responses is about 30 times longer, and the velocity of the waves is about 6-fold smaller, in epithelial versus amoeboid cells. The different kinetics are consistent with the frequency and extension rate of protrusions as well as the speed of movements in the two different cells (Albeck et al., 2013; Aoki et al., 2013; Miao et al., 2019).

4. Novel Characteristics in Human Epithelial Cells

We also observed novel wave characteristics that had not been previously reported. First, we observed switching between travelling and standing waves, a recently predicted feature of excitable systems (Bhattacharya, et al., submitted). We have showed evidence of travelling waves help cell forming protrusions and thus facilitate cell migration. However, we are currently not sure about the potential physiological function of the standing waves. We hypothesize that these standing waves detected in Kras_G12V transformed cells might be able to regulate the formation of invadopodia. It wound be very interesting to have further investigation on this.

Second, we found that uniform growth factor triggered a global response, temporarily overwhelming wave activity, and that local gradients provided a directional bias to the waves in MDA-MB-231 cells. Our observations in MDA-MB-231 were closely simulated by manipulating the threshold in the STEN-CEN computational model. In *Dictyostelium*, the extent to which STEN activity can be biased by external stimuli appears to be context dependent and has been debated (Huang et al., 2013; Gerisch et al., 2016). Our observations provide clear new evidence to support the excitable network hypothesis with respect to cell guidance.

5. Molecular Identity of the Feedback Loops

Our observations lead to a schematic view of the molecular identity of some of the feedback loops that bring about excitability (see Figure 13J). Ras is activated by EGF and in turn activates ERK. ERK negatively regulates Ras activity. It has been reported that Ras activation reduces PI(4,5)P2 (Van Rheenen et al., 2007). We found PI(4,5)P2 is a negative regulator of Ras activity, which would complete a mutually inhibitory positive feedback loop. PI(3,4)P2 as a product of PI(3,4,5)P3

provides negative feedback to Ras. Finally PI(3,4,5)P3 together with mTORC2 provides a link through AKT to the cytoskeleton.

Similar observations were previously made in *Dictyostelium* except that in amoebae resting PI(3,4)P2 levels are high and AKT can serve as a negative regulator of Ras activation. The consistent role of PI(3,4)P2 as a negative regulator in both systems is surprising since PI(3,4)P2 is at the leading edge of the cell and generally considered as a positive regulator (Bae et al., 2010; Hansen et al., 2015). However, our studies (Figure 13A-C) and those in *Dictyostelium* indicate PI(3,4)P2 at the leading edge lags behind PIP3. Many mammalian cancer studies indicated that PI(3,4)P2, similar to PIP3, was a pro-cancer factor (Gewinner et al., 2009; Guo et al., 2016; Malek et al., 2017). Our results suggested that during tumor progression the role of PI(3,4)P2, as a negative regulator of Ras activity, might be more complicated than what has been initially proposed and thus called on more future studies in elucidating the exact involvement of PI(3,4)P2 in cancer.

Other studies have pointed to additional feedback loops not assessed here. For instance, Ras, PI3K, the actin cytoskeleton and cellular adhesion can form a positive feedback loop (Huang et al., 2013; Yang et al., 2018). Negative feedback involving myosin and AKT, as well as membrane tension and mTORC2 have been reported (Sasaki et al., 2007; Houk et al., 2012; Diz-Muñoz et al., 2016; Riggi et al., 2018).

6. Consequence of Excitability in Cell Physiology

That excitability the Ras/PI3K/ERK network controls cellular morphology has important functional consequences in cell physiology. First, in migrating cells, stochastic patches, and waves

of the Ras-PI3K signaling activity drive the cytoskeleton to generate protrusions that allow cells to move in random directions in the absence of directional cues (Huang et al., 2013; Taniguchi et al., 2013). Alterations in the threshold lead to rich dynamics of the signaling network reflected in a wide array of migratory behaviors (Miao et al., 2017). Second, during chemotaxis, due to the sensitivity of excitable systems to small changes in the threshold, shallow chemoattractant gradients can be amplified by the signaling network to drive directed movement in a noisy environment (Tang et al., 2014). Third, the feedback interactions between the proteins provide a mechanism for integrating different stimuli. For example, evidence suggests that mechanical stimuli, which signal through adhesion complexes, and growth hormones, which activate tyrosine kinase receptors, are integrated by modulating feedback loops at different points to regulate the frequency of ERK pulses, which determines cell cycle entry (Yang et al., 2018).

7. A Novel View of Oncogenic Transformation

Excitability of the Ras/PI3K/ERK network has important consequences in cancer. First, the excitable network can generate patterns such as travelling waves of different dimensions or standing waves (Xiong et al., 2010; Bhattacharya et al., submitted). These patterns can generate a large repertoire of protrusions such as pseudopodia, filopodia, lamellipodia, or invadopodia and consequently explain a wide range of migratory behaviors (Huang et al, 2013; Taniguchi et al, 2013; Miao et al., 2017; Miao et al., 2019). Second, we found in Kras transformed cells, as well as in cells where Ras was acutely activated, an increase in the wave and ERK activity, suggesting how these increased activities may control cell proliferation and cancer progression (Roberts et al., 2007; Mebratu et al., 2009; Mendoza et al., 2011; Serra et al., 2011; Samatar et al., 2014; Tanimura

et al., 2017; Yang et al., 2018). Taken together, our studies suggest a novel view of oncogenic transformation as a shift to a lower threshold or set point of the Ras/PI3K/ERK excitable network. This change in threshold is manifested by an increase in stochastic noise driven activities such as the number and the range of propagating waves and the frequency of ERK pulses. The lowering of threshold most likely leads to the increased migration, macropinocytosis, and proliferation of cancer cells and it possibly can be used to assess cancer severity as well as a target for intervention.

8. Future Directions

Besides the Kras and/or MYC transformed cells, it would be interesting to evaluate the cancer phenotypes of other threshold lowered MCF-10A cells, such as PI(4,5)P2 reduced cells. We have some preliminary data indicating Epithelial to Mesenchymal Transition phenotype of PI(4,5)P2 lowered cells. We have also proposed to test the invasion capability of these cells with the trans-well assays, dissemination ability in the 3D organoid, and capability to form tumor in mouse xenografts.

The ERK-KTR sensor we used in our study has very high sensitivity in showing the whole cell level of ERK activation but lacks the subcellular information. It is very important to know whether ERK is also locally coupled with Ras-PI3K-F-actin waves via FRET based local biosensor for ERK.

Cell can use very different mechanism for migration from 2D to 3D conditions (Yamada et al., 2019). Petrie et al. has showed in the 3D extracellular matrices, cell cytoplasm can be divided to forward and rear compartments by its nucleus, and the contractility force generated by actomyosin at the back pulled the nucleus forward and thus changed the pressure between the two

compartments, which contributed to this lamellipodia-independent 3D cell migration (Petrie et al., 2014). The Ras-PI3K-F-actin waves have never been reported in the 3D setting. We would like to see the possibility of detecting these waves in 3D cell culture condition. We are also interested in how the ERK pulse frequency is regulated among the population of a 3D organoid at single cell level. With the ERK-KTR, it does not seem to be too difficult. We would like to know how the ERK pulse frequency of PI(4,5)P2 lowered or Kras transformed MCF10A cells are different to that of the control groups.

Excitability of signaling may be a common mechanism in controlling other biochemical and biophysical processes of cell biology and the initiation and progression of other diseases besides cancer. For instance, electrotaxis is another critical type of directed migration. A former genetic screening in *Dictyostelium* has revealed that these genes involved in electrotaxis are to a very large extent similar to the canonical genes regulating the chemotaxis (Gao et al., 2015). We have some preliminary data showing that Ras-PI3K-F-actin waves in MDA-MB-231 cells can be regulated by DC electric field. It would be of great significance to study whether and how the excitability of the Ras/PI3K/ERK network controls the electrotaxis.

Conclusion

Our studies focused on the systems-level understanding of the intrinsic property of signal transduction networks in controlling cell basic behavior (migration) and human disease progression (cancer transformation). We found that 1) the excitability of signal transduction networks regulates the morphology dynamics and migratory mode transitions, an evolutionarily conserved mechanism from amoeboid *Dictyostelium* cells to human epithelial cells, and 2) cancer cells can be viewed as having a lower threshold state of these excitable networks, a conceptual advance with predictive value.

We demonstrate that traveling waves of Ras and PI3K activation propagate on the basal surfaces of several human mammary epithelial cell lines and drive actin polymerization. Protrusions that mediate cell migration are caused by these Ras-PI3K waves reaching the cell perimeter and the waves can be guided by growth factors showing that they underlie chemotaxis. Besides the traveling waves, the Ras/PI3K/ERK network exhibits other key features of biochemical excitability, including annihilation of oppositely directed waves, all-or-none responsiveness, and refractoriness to repeated stimuli. Abrupt perturbations to Ras activity, PI(4,5)P2, and PI(3,4)P2 lower the threshold for network activation which increases the number and range of propagating waves. Inhibition of TORC2 increases the threshold and reduces the wave and protrusion activity. These observations define the positive and negative feedback loops within the network that underlie excitability. Our demonstration of excitability and wave propagation in the Ras/PI3K/ERK network in human epithelial cells establishes a new mechanism controlling human cell migration.

Importantly, we demonstrate that oncogenic cellular transformation with constitutively activated Ras or Ras/MYC leads to enhanced, and de novo, wave generation. Thus, mutation of an individual component such as Ras shifts the entire Ras/PI3K/ERK network to a lower threshold state of excitability. These changes underlie the aberrant motility consistent with a role in metastasis, and, potentially, changes in gene expression characteristics of oncogenic transformed cells. This new view is likely to motivate further studies on cancer. For example, wave properties may indicate cancer grade, potential interventions might be judged by effects on wave features, and different interventions that alter the threshold may be predicted to have synergistic or antagonistic effects.

Materials and Methods

Cells

MCF-10A cells, acquired from Iijima Lab (Johns Hopkins University), were grown at 37°C in 5% CO2 using DMEM/F-12 medium (Gibco, #10565042) supplemented with 5% horse serum (Gibco, #26050088), 20 ng/ml EGF (Sigma, #E9644), 100 ng/ml cholera toxin (Sigma, #C-8052), 0.5 mg/ml hydrocortisone (Sigma, #H-0888) and 10 μg/ml insulin (Sigma #I-1882). MDA-MB-231 cells, acquired from Liu Lab (JHU), were maintained in DMEM medium (Gibco, #10566024) containing 10% FBS (Gibco, #16140071).

Transient transfections of the cells were performed using Lipofectamine 3000 (Invitrogen, #L3000008) following manufacturer's instructions. Stable transfected cell lines were selected and/or maintained in culture media containing drugs (2 μg/ml Puromycin, ThermoFisher, #A1113803 and/or 2 mg/ml Zeocin, ThermoFisher, #R25001). Some stable cell lines were sorted by fluorescence tags.

Cells were transferred to 35 mm glass-bottom dishes (Mattek, #P35G-0.170-14-C) or chambered coverglass (Lab-Tek, #155409PK) and allowed to attach overnight prior to imaging. Cells were seeded and incubated at 37°C in 5% CO2 overnight before harvest for immunoblotting, immunofluorescence, or live cell imaging.

Plasmids

Constructs of CFP-Lyn-FRB, mCherry-FKBP-Inp54p, mCherry-FKBP-Inp54p (D281A), YFP-FKBP-CDC25, YFP-PH-PLCΔ, and RFP-PH-TAPP1 were obtained from Inoue Lab (JHU).

GFP/RFP-PH-AKT, RFP-LifeAct, pFUW2, pMDL, pRSV, and pCMV were obtained from Desiderio Lab (JHU). Raf-RBD (51-220)-GFP was obtained from Balla Lab (NIH). pLenti-GFP-ERKKTR (#59150), mCherry-FKBP-INPP4B (#116864), mCherry-FKBP-INPP4B (C842A) (#116865), pBABE-KrasG12V (#9052), pBABE-C-MYC (#17758), pBABE-HrasG12V (#9051), pUMVC (#8449), pCMV-VSV-G (#8454), psPAX2 (#12260) and pMD2.G (#12259) constructs were obtained from AddGene. Lyn-FRB, FKBP-Inp54p, FKBP-Inp54p (D281A), PH-PLCΔ, PH-AKT, LifeAct, and RBD were subcloned to lenti-viral expression plasmid pFUW2. The pLKO.1 knock-down plasmids scramble shRNA (#1864), Rictor_#1 shRNA (#1853), Rictor_#2 shRNA (#1854), mTOR_#1 shRNA (#1855), and mTOR_#2 shRNA (#1856) were obtained from AddGene.

Drugs

Stocks of 10 mM PP242 (Sigma, #P0037), 25 mM Latrunculin A (Enzo, #BML-T119-0100), 10 mM Ulixertinib (MedChemExpress, #HY-15816), 50 mM LY294002 (Invitrogen, #PHZ1144), 10 mM ZSTK474 (Cell Signaling, #13213), 25 mM for Latrunculin B (Enzo, #BML-T110-0001), 1 mM Jasplakinolide (Enzo, #ALX-350-275-C050), 10 mM Y-27632 (Enzo, #ALX-270-333-M001) and 10 mM Rapamycin (Cayman, #13346) were prepared by dissolving the chemicals in DMSO. The stocks were diluted to the indicated final concentrations in culture medium or live cell imaging medium. The EGF stock solution was prepared by dissolving EGF (Sigma, #E9644) in 10 mM acetic acid to a final concentration of 1 mg/ml. Insulin (Sigma #I-1882) was resuspended at 10 mg/ml in sterile ddH2O containing 1% glacial acetic acid. Hydrocortisone (Sigma #H-0888) was resuspended at 1 mg/ml in 200 proof ethanol. Cholera toxin (Sigma #C-8052) was resuspended at

1 mg/ml in sterile ddH2O and stored at 4°C. All drug stocks except cholera toxin were stored at -20°C.

Virus Generation

25 ml of 293T cells were seeded at $6x10^5$/ml to 15 cm cell culture dishes on day 1. Conventional calcium phosphate transfection was performed on day 2 to deliver expressing and packaging plasmids into 293T cells. 20 µg pFUW2, 9.375 µg pMDL, 9.375 µg pRSV, 9.375 µg pCMV plasmids (or 10 µg pBABE, 9 µg pUMVC, 1 µg pCMV-VSV-G; or 10 µg pLenti/pLKO.1, 8 µg psPAX2, 2 µg pMD2.G), 250 µl CaCl2 and ddH2O in a total volume of 2.5 ml were mixed with 2.5 ml 2xHEPES (PH=7.05) and incubated for 5 min. The transfection mix was added to the plated cells and shaken gently. Media was changed after 4-6 hours. For virus collection, the medium from infected cells was collected on day 5 and spun at 1000 rpm for 3 min to remove the debris and filtered through 0.45 µm filter followed by ultracentrifugation at 25,000 rpm for 90 min at 4°C in a Beckman ultracentrifuge. The supernatant was discarded and the pellet was dissolved in 70 ul PBS overnight at 4°C to obtain concentrated virus, which was stored as 25 µl aliquots at -80°C.

Immunoblotting

Cells were seeded at $4x10^5$ per well in 6-well plates with appropriate growth medium and incubated at 37°C, 5% CO2 overnight, or treated with drugs for indicated period of time before harvesting. Cell lysates were prepared by cell lysis on ice with 3X RIPA buffer containing protease inhibitors (Roche, #11836170001) and phosphatase inhibitor cocktail (Sigma, #P5726). Immunoblotting of individual protein bands was performed by overnight incubating the PVDF

membranes with the following primary antibodies (all purchased from Cell Signaling) diluted in 1X Odyssey Blocking Buffer (LI-COR, #927-50000): rabbit anti-phospho-ERK (#9101), mouse anti-ERK1/2 (#9107), rabbit anti-phospho-AKT (Ser473) (#4060), mouse anti-AKT (#2920), anti-mTor (#2972), anti-Rictor (#2140), anti-GAPDH (#2118) and rabbit anti-β-Actin (#4970). Fluorescent dyes-conjugated goat anti-rabbit or anti-mouse antibodies (LI-COR, #925-68071 or #925-32210) were used as secondary antibodies to visualize the protein bands with the Odyssey CLx - LI-COR Imaging System.

Immunofluorescence

Cells were seeded on glass bottom imaging dishes or chambers with appropriate growth medium and incubated at 37°C, 5% CO2 overnight before fixation. Rapamycin was added 1 hour before fixation. Cells were fixed with 4% formaldehyde diluted in warm PBS for 15 min at room temperature. Immunostaining was performed by incubating specimen in appropriate primary antibody in dilution buffer (1X PBS/1% BSA/0.3% Triton X-100) overnight at 4°C and in fluorochrome-conjugated secondary antibody in dilution buffer for 2 hours at room temperature in the dark after 3 PBS rinses. Cells were covered with Prolong Gold Antifade Reagent (Cell Signaling, #9071) and TIRF imaging was done within 24 hours. Primary antibodies for AKT and p-AKT S473 are described in immunoblotting session. Secondary antibodies are anti-rabbit IgG_Alexa Fluor® 488 conjugate (Cell Signaling, #4412) and anti-mouse IgG_Alexa Fluor® 488 conjugate (Cell Signaling, #4408). Alexa Fluor® 647 Phalloidin was purchased from Cell Signaling (#8940).

Microscopy

Total internal reflection fluorescence, wide-field epifluorescence, and confocal microscopy have been described previously (Huang et al., 2013). Briefly, epifluorescence and TIRF microscopy experiments were carried out on a Nikon Eclipse TiE microscope illuminated by an Ar laser (GFP) and a diode laser (RFP). Images were acquired by a photometrics Evolve electron Multiplying Charge-Coupled Device camera (EMCCD) camera controlled by Nikon NIS-Elements. Confocal microscopy was carried out on Zeiss AxioObserver inverted microscope with either LSM780-Quasar (34-channel spectral, high-sensitivity gallium arsenide phosphide detectors, GaAsP) or LSM800 confocal module controlled by the Zen software. All live cell imaging was carried out in a temperature/humidity/CO2-regulated chamber.

Computational Modeling

Wave simulations based on excitable system with global and local perturbations

The excitable waves were modeled through reaction-diffusion equations (Xiong et al., 2010). The signal transduction excitable network (STEN) was set up as an activator (X)-inhibitor (Y) system as shown below:

$$\frac{\partial X}{\partial t} = D_X \nabla^2 X - \ (a_1 + a_2(Y - S_{in}))X + \frac{a_3 X^2}{a_4^2 + X^2} + a_5 + U_N$$

$$\frac{\partial Y}{\partial t} = D_Y \nabla^2 Y + \ \varepsilon(-Y + c_1 X)$$

The non-linear term in the first equation contributes to positive feedback while the epsilon (ε) in the second equation creates a delay in the response of the inhibitor. When the activator receives a

supra-threshold stochastic input, the autocatalytic feedback leads to a sharp rise in activity, creating the wave front (green in Figure 4G and 4H). The inhibitor, albeit slowly, accumulates to ultimately subdue the activator concentration – creating the wave back (red in Figure 4G and 4H). After the inhibitor subdues the activator response, it then decays back to resting concentration, resulting in a refractory period. When coupled with diffusion across adjacent excitable elements, this creates a propagating wave.

Simulations were done using a two-dimensional 200x200 array in MATLAB, using stochastic differential equations (Picchini, 2007). The term U_N incorporates the stochastic input to the system which is modeled as a zero-mean Gaussian white noise process (σ). The parameter values used are: $a_1 = 0.167$, $a_2 = 16.67$, $a_3 = 167$, $a_4 = 1.2$, $a_5 = 1.47$, $\varepsilon = 0.12$, $c_1 = 39$, $D_X = 2.2$, and $D_Y = 1.2$.

External stimulus to the excitable system is provided through the term S_{in} in the activator equation. In the absence of a stimulus, this term was set to zero. For a global stimulus, the term was set to 0.2 for the whole 200x200 system. For a gradient simulation, a gaussian profile was used for S_{in}, with mean at the bottom edge of the spatial array, and a standard deviation of 60 – with the amplitude rising from 0 to 0.5.

Bibliography

Adams, C.F., and Paul, A.J. (1999). Phototaxis and Geotaxis of Light-Adapted Zoeae of the Golden King Crab Lithodes aequispinus (Anomura: Lithodidae) in the Laboratory. Journal of Crustacean Biology 19, 106.

Albeck, J.G., Mills, G.B., and Brugge, J.S. (2013). Frequency-modulated pulses of ERK activity transmit quantitative proliferation signals. Mol. Cell 49, 249–261.

Aoki, K., Kumagai, Y., Sakurai, A., Komatsu, N., Fujita, Y., Shionyu, C., and Matsuda, M. (2013). Stochastic ERK activation induced by noise and cell-to-cell propagation regulates cell density-dependent proliferation. Mol. Cell 52, 529–540.

Arai, Y., Shibata, T., Matsuoka, S., Sato, M.J., Yanagida, T., and Ueda, M. (2010). Self-organization of the phosphatidylinositol lipids signaling system for random cell migration. Proc. Natl. Acad. Sci. U. S. A. 107, 12399–12404.

Armitage JP, Hellingwerf KJ. (2003). Light-induced behavioral responses ('phototaxis') in prokaryotes. Photosynth. Res. 76:145–55

Bae, Y.H., Ding, Z., Das, T., Wells, A., Gertler, F., and Roy, P. (2010). Profilin1 regulates PI (3, 4) P2 and lamellipodin accumulation at the leading edge thus influencing motility of MDA-MB-231 cells. Proceedings of the National Academy of Sciences 107, 21547–21552.

Bagorda, A., and Parent, C.A. (2008). Eukaryotic chemotaxis at a glance. J. Cell Sci. 121, 2621–2624.

Barnhart, E.L., Allen, G.M., Jülicher, F., and Theriot, J.A. (2010). Bipedal locomotion in crawling cells. Biophys. J. 98, 933–942.

Basolo, F., Elliott, J., Tait, L., Chen, X.Q., Maloney, T., Russo, I.H., Pauley, R., Momiki, S., Caamano, J., Klein-Szanto, A.J.P., et al. (1991). Transformation of human breast epithelial cells by c-Ha-ras oncogene. Mol. Carcinog. 4, 25–35.

Baumann, K. (2014). Stem cells: moving out of the niche. Nat. Rev. Mol. Cell Biol. 15, 79.

Beloussov, L.V., Louchinskaia, N.N., and Stein, A.A. (2000). Tension-dependent collective cell movements in the early gastrula ectoderm of Xenopus laevis embryos. Dev. Genes Evol. 210, 92–104.

Bement, W.M., Leda, M., Moe, A.M., Kita, A.M., Larson, M.E., Golding, A.E., Pfeuti, C., Su, K.-C., Miller, A.L., Goryachev, A.B., et al. (2015). Activator-inhibitor coupling between Rho signalling and actin assembly makes the cell cortex an excitable medium. Nat. Cell Biol. 17, 1471–1483.

Blaser, H., Reichman-Fried, M., Castanon, I., Dumstrei, K., Marlow, F.L., Kawakami, K., Solnica-Krezel, L., Heisenberg, C.-P., and Raz, E. (2006). Migration of zebrafish primordial germ cells: a role for myosin contraction and cytoplasmic flow. Dev. Cell 11, 613–627.

Bray, D. (2000). Cell movements: from molecules to motility (Garland Science).

Carter, S.B. (1965). Principles of Cell Motility: The Direction of Cell Movement and Cancer Invasion. Nature 208, 1183–1187.

Case, L.B., and Waterman, C.M. (2011). Adhesive F-actin waves: a novel integrin-mediated adhesion complex coupled to ventral actin polymerization. PLoS One 6, e26631.

Condeelis, J., Singer, R.H., and Segall, J.E. (2005). The great escape: when cancer cells hijack the genes for chemotaxis and motility. Annu. Rev. Cell Dev. Biol. 21, 695–718.

Corcoran, R.B., Ebi, H., Turke, A.B., Coffee, E.M., Nishino, M., Cogdill, A.P., Brown, R.D., Della Pelle, P., Dias-Santagata, D., Hung, K.E., et al. (2012). EGFR-Mediated Reactivation of MAPK Signaling Contributes to Insensitivity of BRAF -Mutant Colorectal Cancers to RAF Inhibition with Vemurafenib. Cancer Discovery 2, 227–235.

Cortese, B., Gigli, G., and Riehle, M. (2009). Mechanical Gradient Cues for Guided Cell Motility and Control of Cell Behavior on Uniform Substrates. Adv. Funct. Mater. 19, 2961–2968.

Cortese, B., Palamà, I.E., D'Amone, S., and Gigli, G. (2014). Influence of electrotaxis on cell behaviour. Integr. Biol. 6, 817–830.

Cortese, B., Piliego, C., Viola, I., D'Amone, S., Cingolani, R., and Gigli, G. (2009). Engineering Transfer of Micro- and Nanometer-Scale Features by Surface Energy Modification. Langmuir 25, 7025–7031.

Curtis, A.S.G., Casey, B., Gallagher, J.O., Pasqui, D., Wood, M.A., and Wilkinson, C.D.W. (2001). Substratum nanotopography and the adhesion of biological cells. Are symmetry or regularity of nanotopography important? Biophysical Chemistry 94, 275–283.

Dalby, M.J., Gadegaard, N., Tare, R., Andar, A., Riehle, M.O., Herzyk, P., Wilkinson, C.D.W., and Oreffo, R.O.C. (2007). The control of human mesenchymal cell differentiation using nanoscale symmetry and disorder. Nat. Mater. 6, 997–1003.

Devreotes, P.N., Bhattacharya, S., Edwards, M., Iglesias, P.A., Lampert, T., and Miao, Y. (2017). Excitable Signal Transduction Networks in Directed Cell Migration. Annu. Rev. Cell Dev. Biol. 33, 103–125.

Diz-Muñoz, A., Thurley, K., Chintamen, S., Altschuler, S.J., Wu, L.F., Fletcher, D.A., and Weiner, O.D. (2016). Membrane Tension Acts Through PLD2 and mTORC2 to Limit Actin Network Assembly During Neutrophil Migration. PLOS Biology 14, e1002474.

Erickson, C.A., and Nuccitelli, R. (1984). Embryonic fibroblast motility and orientation can be influenced by physiological electric fields. J. Cell Biol. 98, 296–307.

Fackler, O.T., and Grosse, R. (2008). Cell motility through plasma membrane blebbing. J. Cell Biol. 181, 879–884.

Gao, R., Zhao, S., Jiang, X., Sun, Y., Zhao, S., Gao, J., Borleis, J., Willard, S., Tang, M., Cai, H., et al. (2015). A large-scale screen reveals genes that mediate electrotaxis in Dictyostelium discoideum. Sci. Signal. 8, ra50.

Gao, R.-C., Zhang, X.-D., Sun, Y.-H., Kamimura, Y., Mogilner, A., Devreotes, P.N., and Zhao, M. (2011). Different roles of membrane potentials in electrotaxis and chemotaxis of dictyostelium cells. Eukaryot. Cell 10, 1251–1256.

Gerisch, G., and Ecke, M. (2016). Wave Patterns in Cell Membrane and Actin Cortex Uncoupled from Chemotactic Signals. Methods Mol. Biol. 1407, 79–96.

Gerisch, G., Bretschneider, T., Müller-Taubenberger, A., Simmeth, E., Ecke, M., Diez, S., and Anderson, K. (2004). Mobile actin clusters and traveling waves in cells recovering from actin depolymerization. Biophys. J. 87, 3493–3503.

Gewinner, C., Wang, Z.C., Richardson, A., Teruya-Feldstein, J., Etemadmoghadam, D., Bowtell, D., Barretina, J., Lin, W.M., Rameh, L., Salmena, L., et al. (2009). Evidence that inositol polyphosphate 4-phosphatase type II is a tumor suppressor that inhibits PI3K signaling. Cancer Cell 16, 115–125.

Goulden, B.D., Pacheco, J., Dull, A., Zewe, J.P., Deiters, A., and Hammond, G.R.V. (2019). A high-avidity biosensor reveals plasma membrane PI(3,4)P2 is predominantly a class I PI3K signaling product. J. Cell Biol. 218, 1066–1079.

Guo, S.T., Chi, M.N., Yang, R.H., Guo, X.Y., Zan, L.K., Wang, C.Y., Xi, Y.F., Jin, L., Croft, A., Tseng, H.-Y., et al. (2016). INPP4B is an oncogenic regulator in human colon cancer. Oncogene 35, 3049–3061.

Hale, N.A., Yang, Y., and Rajagopalan, P. (2010). Cell migration at the interface of a dual chemical-mechanical gradient. ACS Appl. Mater. Interfaces 2, 2317–2324.

Hansen, S.D., and Dyche Mullins, R. (2015). Lamellipodin promotes actin assembly by clustering Ena/VASP proteins and tethering them to actin filaments. ELife 4.

Hawkins, P.T., and Stephens, L.R. (2016). Emerging evidence of signalling roles for PI (3, 4) P2 in Class I and II PI3K-regulated pathways. Biochem. Soc. Trans. 44, 307–314.

Helmick, L., de Mayolo, A.A., Zhang, Y., Cheng, C.-M., Watkins, S.C., Wu, C., and LeDuc, P.R. (2008). Spatiotemporal Response of Living Cell Structures inDictyostelium discoideumwith Semiconductor Quantum Dots. Nano Letters 8, 1303–1308.

Houk, A.R., Jilkine, A., Mejean, C.O., Boltyanskiy, R., Dufresne, E.R., Angenent, S.B., Altschuler, S.J., Wu, L.F., and Weiner, O.D. (2012). Membrane tension maintains cell polarity by confining signals to the leading edge during neutrophil migration. Cell 148, 175–188.

Huang, C.-H., Tang, M., Shi, C., Iglesias, P.A., and Devreotes, P.N. (2013). An excitable signal integrator couples to an idling cytoskeletal oscillator to drive cell migration. Nat. Cell Biol. 15, 1307–1316.

Imbalzano, K.M., Tatarkova, I., Imbalzano, A.N., and Nickerson, J.A. (2009). Increasingly transformed MCF-10A cells have a progressively tumor-like phenotype in three-dimensional basement membrane culture. Cancer Cell Int. 9, 7.

Inagaki, N., and Katsuno, H. (2017). Actin waves: origin of cell polarization and migration? Trends Cell Biol. 27, 515–526.

Jeon, N.L., Baskaran, H., Dertinger, S.K.W., Whitesides, G.M., Van De Water, L., and Toner, M. (2002). Neutrophil chemotaxis in linear and complex gradients of interleukin-8 formed in a microfabricated device. Nature Biotechnology 20, 826–830.

Keren, K., and Theriot, J.A. (2008). Biophysical Aspects of Actin-Based Cell Motility in Fish Epithelial Keratocytes. In Cell Motility, P. Lenz, ed. (New York, NY: Springer New York), pp. 31–58.

Lakshman, R., and Finn, A. (2001). Neutrophil disorders and their management. J. Clin. Pathol. 54, 7–19.

Lam Hui, K., Kwak, S.I., and Upadhyaya, A. (2014). Adhesion-dependent modulation of actin dynamics in Jurkat T cells. Cytoskeleton 71, 119–135.

Lito, P., Rosen, N., and Solit, D.B. (2013). Tumor adaptation and resistance to RAF inhibitors. Nat. Med. 19, 1401–1409.

Liu, M., Casimiro, M.C., Wang, C., Shirley, L.A., Jiao, X., Katiyar, S., Ju, X., Li, Z., Yu, Z., Zhou, J., et al. (2009). p21CIP1 attenuates Ras- and c-Myc-dependent breast tumor epithelial mesenchymal transition and cancer stem cell-like gene expression in vivo. Proc. Natl. Acad. Sci. U. S. A. 106, 19035–19039.

Lo, C.M., Wang, H.B., Dembo, M., and Wang, Y.L. (2000). Cell movement is guided by the rigidity of the substrate. Biophys. J. 79, 144–152.

Malek, M., Kielkowska, A., Chessa, T., Anderson, K.E., Barneda, D., Pir, P., Nakanishi, H., Eguchi, S., Koizumi, A., Sasaki, J., et al. (2017). PTEN Regulates PI(3,4)P2 Signaling Downstream of Class I PI3K. Mol. Cell 68, 566–580.e10.

Manahan, C.L., Iglesias, P.A., Long, Y., and Devreotes, P.N. (2004). Chemoattractant signaling in Dictyostelium discoideum. Annu. Rev. Cell Dev. Biol. 20, 223–253.

Marchesin, V., Montagnac, G., and Chavrier, P. (2015). ARF6 promotes the formation of Rac1 and WAVE-dependent ventral F-actin rosettes in breast cancer cells in response to epidermal growth factor. PLoS One 10, e0121747.

Martinko A.J., Truillet C., Julien O., Diaz J.E., Horlbeck M.A., Whiteley G., Blonder J., Weissman J.S., Bandyopadhyay S., Evans M.J., et al. (2018). Targeting RAS-driven human cancer cells with antibodies to upregulated and essential cell-surface proteins. Elife 7, e31098.

Mebratu, Y., and Tesfaigzi, Y. (2009). How ERK1/2 activation controls cell proliferation and cell death: Is subcellular localization the answer? Cell Cycle 8, 1168–1175.

Mendoza, M.C., Er, E.E., Zhang, W., Ballif, B.A., Elliott, H.L., Danuser, G., and Blenis, J. (2011). ERK-MAPK drives lamellipodia protrusion by activating the WAVE2 regulatory complex. Mol. Cell 41, 661–671.

Miao, Y., Bhattacharya, S., Banerjee, T., Abubaker-Sharif, B., Long, Y., Inoue, T., Iglesias, P.A., and Devreotes, P.N. (2019). Wave patterns organize cellular protrusions and control cortical dynamics. Mol. Syst. Biol. 15, e8585.

Miao, Y., Bhattacharya, S., Edwards, M., Cai, H., Inoue, T., Iglesias, P.A., and Devreotes, P.N. (2017). Altering the threshold of an excitable signal transduction network changes cell migratory modes. Nat. Cell Biol. 19, 329–340.

Moulding, D.A., Record, J., Malinova, D., and Thrasher, A.J. (2013). Actin cytoskeletal defects in immunodeficiency. Immunol. Rev. 256, 282–299.

Neumann, N.M., Perrone, M.C., Veldhuis, J.H., Huebner, R.J., Zhan, H., Devreotes, P.N., Brodland, G.W., and Ewald, A.J. (2018). Coordination of Receptor Tyrosine Kinase Signaling and Interfacial Tension Dynamics Drives Radial Intercalation and Tube Elongation. Dev. Cell 45, 67–82.e6.

Nishikawa, M., Hörning, M., Ueda, M., and Shibata, T. (2014). Excitable signal transduction induces both spontaneous and directional cell asymmetries in the phosphatidylinositol lipid signaling system for eukaryotic chemotaxis. Biophys. J. 106, 723–734.

Palamà, I.E., D'Amone, S., Coluccia, A.M.L., Biasiucci, M., and Gigli, G. (2012). Cell self-patterning on uniform PDMS-surfaces with controlled mechanical cues. Integr. Biol. 4, 228–236.

Peng, G.E., Wilson, S.R., and Weiner, O.D. (2011). A pharmacological cocktail for arresting actin dynamics in living cells. Mol. Biol. Cell 22, 3986–3994.

Petrie, R.J., Koo, H., and Yamada, K.M. (2014). Generation of compartmentalized pressure by a nuclear piston governs cell motility in a 3D matrix. Science 345, 1062–1065.

Picchini, U. (2007). SDE Toolbox: Simulation and estimation of stochastic differential equations with MATLAB.

Prahallad, A., Sun, C., Huang, S., Di Nicolantonio, F., Salazar, R., Zecchin, D., Beijersbergen, R.L., Bardelli, A., and Bernards, R. (2012). Unresponsiveness of colon cancer to BRAF(V600E) inhibition through feedback activation of EGFR. Nature 483, 100–103.

Ramot, D., MacInnis, B.L., Lee, H.-C., and Goodman, M.B. (2008). Thermotaxis is a robust mechanism for thermoregulation in Caenorhabditis elegans nematodes. J. Neurosci. 28, 12546–12557.

Regot, S., Hughey, J.J., Bajar, B.T., Carrasco, S., and Covert, M.W. (2014). High-sensitivity measurements of multiple kinase activities in live single cells. Cell 157, 1724–1734.

Reymond, N., d'Água, B.B., and Ridley, A.J. (2013). Crossing the endothelial barrier during metastasis. Nat. Rev. Cancer 13, 858–870.

Richardson, B.E., and Lehmann, R. (2010). Mechanisms guiding primordial germ cell migration: strategies from different organisms. Nat. Rev. Mol. Cell Biol. 11, 37–49.

Riggi, M., Niewola-Staszkowska, K., Chiaruttini, N., Colom, A., Kusmider, B., Mercier, V., Soleimanpour, S., Stahl, M., Matile, S., Roux, A., et al. (2018). Decrease in plasma membrane

tension triggers PtdIns(4,5)P2 phase separation to inactivate TORC2. Nature Cell Biology 20, 1043–1051.

Roberts, P.J., and Der, C.J. (2007). Targeting the Raf-MEK-ERK mitogen-activated protein kinase cascade for the treatment of cancer. Oncogene 26, 3291–3310.

Samatar, A.A., and Poulikakos, P.I. (2014). Targeting RAS–ERK signalling in cancer: promises and challenges. Nat. Rev. Drug Discov. 13, 928.

Saranak, J., and Foster, K.W. (1997). Rhodopsin guides fungal phototaxis. Nature 387, 465–466.

Sasaki, A.T., Janetopoulos, C., Lee, S., Charest, P.G., Takeda, K., Sundheimer, L.W., Meili, R., Devreotes, P.N., and Firtel, R.A. (2007). G protein–independent Ras/PI3K/F-actin circuit regulates basic cell motility. J. Cell Biol. 178, 185–191.

Serra, V., Scaltriti, M., Prudkin, L., Eichhorn, P.J.A., Ibrahim, Y.H., Chandarlapaty, S., Markman, B., Rodriguez, O., Guzman, M., Rodriguez, S., et al. (2011). PI3K inhibition results in enhanced HER signaling and acquired ERK dependency in HER2-overexpressing breast cancer. Oncogene 30, 2547–2557.

Shaw, T.J., and Martin, P. (2009). Wound repair at a glance. J. Cell Sci. 122, 3209–3213.

Shin, S.-Y., -Y. Shin, S., Rath, O., -M. Choo, S., Fee, F., McFerran, B., Kolch, W., and -H. Cho, K. (2009). Positive- and negative-feedback regulations coordinate the dynamic behavior of the Ras-Raf-MEK-ERK signal transduction pathway. Journal of Cell Science 122, 425–435.

Simanshu, D.K., Nissley, D.V., and McCormick, F. (2017). RAS Proteins and Their Regulators in Human Disease. Cell 170, 17–33.

Sparta, B., Pargett, M., Minguet, M., Distor, K., Bell, G., and Albeck, J.G. (2015). Receptor level mechanisms are required for epidermal growth factor (EGF)-stimulated extracellular signal-regulated kinase (ERK) activity pulses. J. Biol. Chem. 290, 24784–24792.

Swaney, K.F., Huang, C.-H., and Devreotes, P.N. (2010). Eukaryotic chemotaxis: a network of signaling pathways controls motility, directional sensing, and polarity. Annu. Rev. Biophys. 39, 265–289.

Tang, M., Wang, M., Shi, C., Iglesias, P.A., Devreotes, P.N., and Huang, C.-H. (2014). Evolutionarily conserved coupling of adaptive and excitable networks mediates eukaryotic chemotaxis. Nature Communications 5.

Taniguchi, D., Ishihara, S., Oonuki, T., Honda-Kitahara, M., Kaneko, K., and Sawai, S. (2013). Phase geometries of two-dimensional excitable waves govern self-organized morphodynamics of amoeboid cells. Proc. Natl. Acad. Sci. U. S. A. 110, 5016–5021.

Tanimura, S., and Takeda, K. (2017). ERK signalling as a regulator of cell motility. J. Biochem. 162, 145–154.

Tessier-Lavigne, M. (1994). Axon guidance by diffusible repellants and attractants. Curr. Opin. Genet. Dev. 4, 596–601.

Van Rheenen, J., Song, X., Van Roosmalen, W., Cammer, M., Chen, X., DesMarais, V., Yip, S.-C., Backer, J.M., Eddy, R.J., and Condeelis, J.S. (2007). EGF-induced PIP2 hydrolysis releases and activates cofilin locally in carcinoma cells. J. Cell Biol. 179, 1247–1259.

Vicker, M.G. (2002). F-actin assembly in Dictyostelium cell locomotion and shape oscillations propagates as a self-organized reaction--diffusion wave. FEBS Lett. 510, 5–9.

Wang, M.-J., Artemenko, Y., Cai, W.-J., Iglesias, P.A., and Devreotes, P.N. (2014). The directional response of chemotactic cells depends on a balance between cytoskeletal architecture and the external gradient. Cell Rep. 9, 1110–1121.

Weiner, O.D., Marganski, W.A., Wu, L.F., Altschuler, S.J., and Kirschner, M.W. (2007). An actin-based wave generator organizes cell motility. PLoS Biology 5, e221.

Welf, E.S., Ahmed, S., Johnson, H.E., Melvin, A.T., and Haugh, J.M. (2012). Migrating fibroblasts reorient directionality by a metastable, PI3K-dependent mechanism. J. Cell Biol. 197, 105–114.

Whitaker, B.D., and Poff, K.L. (1980). Thermal adaptation of thermosensing and negative thermotaxis in Dictyostelium. Exp. Cell Res. 128, 87–93.

Winans, A.M., Collins, S.R., and Meyer, T. (2016). Waves of actin and microtubule polymerization drive microtubule-based transport and neurite growth before single axon formation. Elife 5, e12387.

Wolf, K., Mazo, I., Leung, H., Engelke, K., von Andrian, U.H., Deryugina, E.I., Strongin, A.Y., Bröcker, E.-B., and Friedl, P. (2003). Compensation mechanism in tumor cell migration: mesenchymal-amoeboid transition after blocking of pericellular proteolysis. J. Cell Biol. 160, 267–277.

Wozniak, M.A., Kwong, L., Chodniewicz, D., Klemke, R.L., and Keely, P.J. (2005). R-Ras controls membrane protrusion and cell migration through the spatial regulation of Rac and Rho. Mol. Biol. Cell 16, 84–96.

Wright, D.E., Wagers, A.J., Gulati, A.P., Johnson, F.L., and Weissman, I.L. (2001). Physiological migration of hematopoietic stem and progenitor cells. Science 294, 1933–1936.

Wu, Z., Su, M., Tong, C., Wu, M., and Liu, J. (2018). Membrane shape-mediated wave propagation of cortical protein dynamics. Nat. Commun. 9, 136.

Xiong, Y., Huang, C.-H., Iglesias, P.A., and Devreotes, P.N. (2010). Cells navigate with a local-excitation, global-inhibition-biased excitable network. Proceedings of the National Academy of Sciences 107, 17079–17086.

Xue, J.Y., Zhao, Y., Aronowitz, J., Mai, T.T., Vides, A., Qeriqi, B., Kim, D., Li, C., de Stanchina, E., Mazutis, L., et al. (2020). Rapid non-uniform adaptation to conformation-specific KRAS(G12C) inhibition. Nature 577, 421–425.

Yamada, K.M., and Sixt, M. (2019). Mechanisms of 3D cell migration. Nat. Rev. Mol. Cell Biol. 20, 738–752.

Yang, H.W., Collins, S.R., and Meyer, T. (2016). Locally excitable Cdc42 signals steer cells during chemotaxis. Nat. Cell Biol. 18, 191–201.

Yang, J.-M., Bhattacharya, S., West-Foyle, H., Hung, C.-F., Wu, T.-C., Iglesias, P.A., and Huang, C.-H. (2018). Integrating chemical and mechanical signals through dynamic coupling between cellular protrusions and pulsed ERK activation. Nat. Commun. 9, 4673.

Ye, X., Chan, K.C., Waters, A.M., Bess, M., Harned, A., Wei, B.R., Loncarek, J., Luke, B.T., Orsburn, B.C., Hollinger, B.D. et al. (2016). Comparative proteomics of a model MCF10A-KRasG12V cell line reveals a distinct molecular signature of the KRasG12V cell surface. Oncotarget, 7(52), p.86948.

Yoshida, K., and Soldati, T. (2006). Dissection of amoeboid movement into two mechanically distinct modes. J. Cell Sci. 119, 3833–3844.

Zhao, M., Song, B., Pu, J., Wada, T., Reid, B., Tai, G., Wang, F., Guo, A., Walczysko, P., Gu, Y., et al. (2006). Electrical signals control wound healing through phosphatidylinositol-3-OH kinase-gamma and PTEN. Nature 442, 457–460.

CURRICULUM VITAE FOR Ph.D. CANDIDATES

The Johns Hopkins University School of Medicine

Huiwang Zhan January 29th, 2020

Educational History

Ph.D. expected	2020	Program in Biological Chemistry	Johns Hopkins School of Medicine
		Mentors: Peter N. Devreotes, PhD and Chuan-Hsiang Huang, MD-PhD	
B.S.	2012	Biological Science	Xiamen University

Other Professional Experiences

Research Rotation	2013.04-2013.12	Lab of Gregg Semenza, JHMI
Research Rotation	2012.12-2013.03	Lab of Richard Huganir, JHMI
Research Rotation	2012.09-2012.11	Lab of Pierre Coulombe, JHSPH

Scholarships, Fellowships, or Other External Funding

N/A

Academic and Other Honors

2018 Travel Award Graduate Student Associate of JHMI

Publications

Zhan H, Bhattacharya S, Cai H, Iglesias PA, Huang CH, Devreotes PN (2020) Migratory transitions and oncogenic transformation in epithelial cells are controlled by the threshold of the Ras/PI3K/ERK excitable network. *Developmental Cell,* In revision.

Bhattacharya S, Banerjee T, Miao Y, **Zhan H**, Devreotes PN, Iglesias PA (2020) Traveling and standing waves mediate pattern formation in cellular protrusions. *Science Advances,* In revision.

Neumann NM, Perrone MC, Veldhuis JH, Huebner RJ, **Zhan H**, Devreotes PN, Brodland GW, Ewald AJ (2018) Coordination of receptor tyrosine kinase signaling and interfacial tension dynamics drives radial intercalation and tube elongation. *Developmental Cell* 45(1):67-82.

Cai Z, Luo W, **Zhan H**, Semenza GL (2013) Hypoxia-inducible factor 1 is required for remote ischemic preconditioning of the heart. *Proceedings of the National Academy of Sciences* 110(43):17462-7.

Song W, Shen D, Kang J, Li S, **Zhan H**, Shi Y, Xiong Y, Liang G, Chen Q (2012) Apoptosis of human cholangiocarcinoma cells induced by ESC-3 from Crocodylus siamensis bile. *World Journal of Gastroenterology: WJG* 18(7):704.

Posters and Abstracts

Zhan H, Bhattacharya S, Cai H, Iglesias PA, Huang CH, Devreotes PN (2019) Excitability of the Ras-PI3K network controls the dynamic morphology and transformation in epithelial cells. ASCB Annual Meeting, Watshington, DC, December 07, 2019.

Zhan H, Bhattacharya S, Cai H, Iglesias PA, Huang CH, Devreotes PN (2019) Cancer cell has lowered threshold of signaling transduction excitable network controlled by PIP-Ras interaction. The Biophysical Society Annual Meeting, Baltimore, MD, March 02, 2019.

Zhan H, Bhattacharya S, Cai H, Iglesias PA, Huang CH, Devreotes PN (2019) A novel view of cancer migration and oncogenic transformation. Gordon Research Conference on Directed Cell Migration, Galveston, TX, January 20, 2019.

etc.

Inventions, Patents, and Copyrights

N/A

Service and Leadership

2015, 16, 17, 18 & 19 Teaching Assistant, Cell Physiology Course for Medical Student, JHMI

2016-2018 Executive Board Member, Co-director for Alumni Relationship, Hopkins Biotech Network

2016-2018 Executive Board Member, Representative of BC Program, Graduate Student Association, JHMI

2014 Program Facilitator, The National Youth Leadership Forum in Medicine, Washington DC Session